UNIVERSITY OF CALGARY

Characterizing intrinsic and stratigraphic Q in VSP data with information measures

by

Siming Lv

A DISSERTATION

SUBMITTED TO THE FACULTY OF GRADUATE STUDIES

IN PARTIAL FULFILLMENT OF THE REQUIREMENTS FOR THE

DEGREE OF MASTER OF SCIENCE

GRADUATE PROGRAM IN GEOLOGY AND GEOPHYSICS

CALGARY, ALBERTA

December, 2017

Abstract

Short-period multiples in finely layered geological media modify a seismic pulse as it propagates. This effect, called stratigraphic filtering, or extrinsic attenuation, is characterized by strong attenuation and dispersion of seismic amplitudes. It is similar to, and in fact very difficult to distinguish from, the effect produced by processes of seismic amplitude loss due to friction (or intrinsic attenuation). This is an important and difficult fact for interpreters of seismic data, because it means that similar data signatures are produced by very different geological and petrophysical features of the Earth. In this thesis I seek data analysis methods with the ability to amplify small differences produced by the processes of intrinsic attenuation and stratigraphic filtering, with the aim of discriminating between the two. In a zero-offset vertical seismic profiling (VSP) data set, at any instant in time we have access to a snapshot of the seismic wavefield along the principal direction of wave propagation. In practice, such a snapshot has the form of discrete amplitude values being assigned to each of a set of discrete depth values. Regarding this snapshot as a "message", made up of a sequence of "letters", or amplitude values, drawn from an "alphabet" of allowable amplitudes, permits the data to be analyzed using information-theoretic methods. For instance, Shannon entropy, which measures the degree of disorder within a message, can be assigned to each snapshot, and the time evolution of this number can be determined directly from a VSP data set. It is hypothesized that processes of intrinsic and extrinsic attenuation cause significant and measurable differences in the evolution of the entropy, which means this information measure could be utilized to help distinguish between the two. I analyze this with synthetic VSPs based on real well-log data, pointing out the important role of amplitude bin size in this information measure and the variability of results that should be expected as bin size changes. I point out with these examples that intrinsic and extrinsic attenuation processes tend to have opposite influences on entropy versus time curves. A field data set example is suggestive that the relative strength of stratigraphic filtering and intrinsic attenuation can be estimated in this way.

Acknowledgements

I extend my sincere appreciation to my supervisor Dr. Kris Innanen for enlightening me with great ideas and continuously providing support during the last two years. He is not only an outstanding scholar but also a responsible teacher that always inspires me to higher pursuits in academia.

I want to thank David Henley, research geophysicist at CREWES, who helped me proofreading this work and gave me lots of useful advice.

Other than that, I want to thank all staff and students in CREWES. They are nice and supportive and we spent a lot of wonderful times together. I especially give my thanks to Laura Baird, the program manager of CREWES, who arranges everything for us, and is so optimistic. She brought a lot of joy to my research life.

Finally, I would like to thank CREWES sponsors and NSERC for their financial support.

Dedication

I dedicate this work to my dear parents Daoping Lv, Wenjun Yang, and my boyfriend Xi Liu.

Table of Contents

List of Tables

List of Figures and Illustrations

List of Symbols, Abbreviations and Nomenclature

Symbol	Definition
CREWES	Consortium for Research in Elastic Wave Exploration Seismology
VSP	Vertical Seismic Profile
Q	Quality factor
2D	Two-dimension
PDF	Probability distribution function
S/N ratio	Signal to noise ratio
P-wave	Compressional wave
S-wave	Shear wave
P-velocity	Compressional wave velocity
IM	Internal multiple
CA	Cumulative attenuation
TL	Transmission loss
H	Shannon Entropy
v	Velocity
ρ	Density
f	Frequency
z	Depth
R	Reflection coefficient
B_x	Cumulative attenuation
G_x	Geometric factor
k_x	Interval/local attenuation
α_x	Interval/local attenuation
u	Wave displacement/amplitude

Chapter 1

INTRODUCTION

1.1 Stratigraphic filtering

1.1.1 Definition

In seismic exploration, when an incident wave traverses a layered sequence, a complex series of interbed multiples is excited. In the case that the layered sequence is nonresolvable by the wavelet (i.e. the wavelet length is larger than the average depth of layers), events called short-term multiples are generated. Among them, the two-bounce, short-term multiples arouse the most interest because they follow closely the main lobe of the first arrival and cause superposition of their energy, which complicates seismic analysis regarding first arrival or multiples. Figure 1.1 illustrates the generation of the two-bounce short-term multiples. In the bottom panel showing the transmitted wave, summation of the short-term multiples produces strong energy that tends to overwhelm the first arrival energy and alter the event distribution.

It has been verified by many experiments and observations that these short-term multiples have attenuating and dispersive effects on the transmitted wave which highly resemble those caused by absorption O'Doherty and Anstey (1971) . They both result in a decayed and spreaded waveform of the seismic wave, in which the high-frequency content of the initial disturbance is reduced and an incoherent coda is appended to the signal (figure 1.2). Some researchers began calling the amplitude attenuation and dispersion caused by the short-term multiples "stratigraphic filtering" because they act like a low-pass filter on seismic waves (Spencer et al., 1977; Banik et al., 1985). My research considers stratigraphic filtering as an extrinsic Q factor in contrast to intrinsic Q (absorption) (find definition of absorption in appendix A), since its mechanism lies in subsurface stratification instead of intrinsic rock properties.

The mechanisms of short-term multiple attenuation and absorption are very different, however. Summation of short-term multiples superposes an appending wave energy to the later part of the first arrival. Also, the high frequency components of the wave are more scattered and delayed by multiples than low frequency components because they see more detailed structures of the media. These broaden the waveform and shift its dominant frequency to a smaller value. In contrast, absorption broadens the first arrival waveform by transforming more energy stored in high frequency components into heat in an irreversible manner.

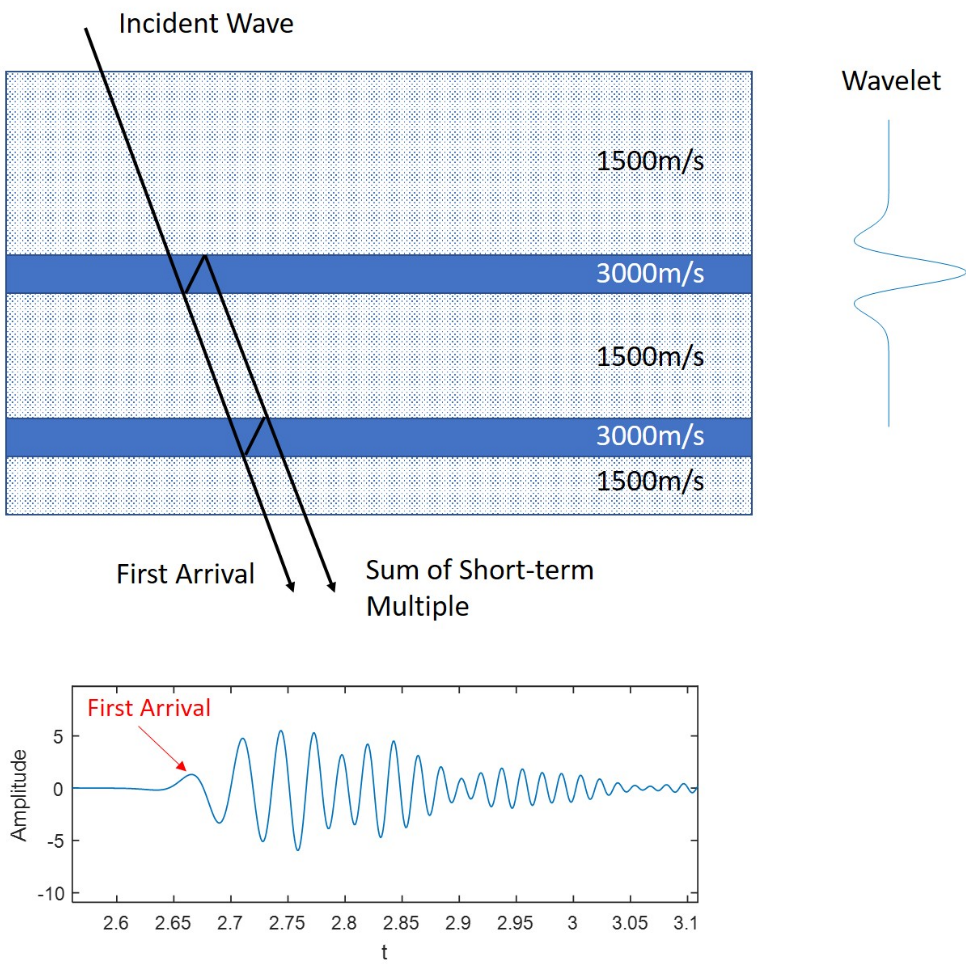

Figure 1.1: A demonstration of the generation of two-bounce, short-term multiples.

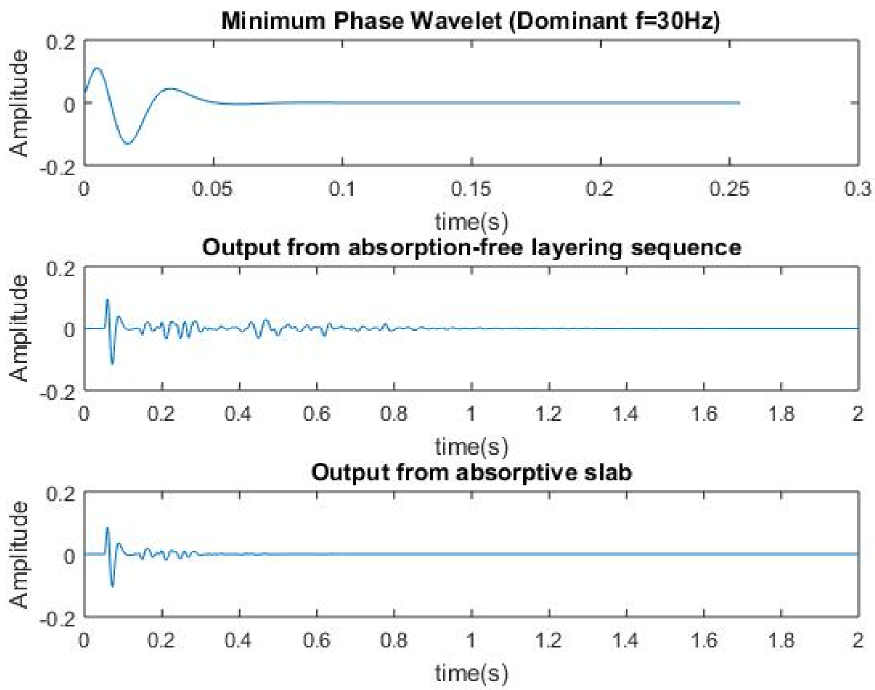

Figure 1.2: Transmitted waves from respectively an absorptive-free layering sequence and an absorptive slab when the normal incident wave is a 30Hz minimum phase wavelet. Noticing the highly similar amplitude attenuating and dispersive effects of stratigraphic filtering and absorption.

1.1.2 Previous work

Geophysicists' attention to stratigraphic filtering was first drawn by the fact that discrepancy exists between the traveltimes of events in seismic and as predicted by well logs; wave amplitudes are frequency-dependent attenuated and dispersed in sedimentary layers, etc. (Trorey, 1962; Resnick, 1990). In fact, both absorption and stratigraphic filtering account for these effects. O'Doherty and Anstey (1971) led the study on stratigraphic filtering: they pointed out the equivalent importance of stratigraphic attenuation and absorptive attenuation in periodically layered media and proposed a mathematical approach to predict the power spectrum of a transmitted wave from reflection coefficient series. Studies to verify their point soon followed (Schoenberger and Levin, 1974, 1978; Stewart et al., 1984; Banik et al., 1985).

In the meantime, significant effort has been expended in developing methods which attempt to distinguish between intrinsic and extrinsic Q; by utilizing the non-linear frequency-dependent attribute of extrinsic Q against linear dependence of intrinsic Q (Spencer et al., 1977), by Q estimation methods (Spencer et al., 1982; Hauge, 1981) or by investigating the amplitude and phase spectra of the transmitted wave (Richards and Menke, 1983). In a recent work, Margrave (2017) estimated intrinsic Q variation in a real zero-offset VSP data with spectral ratio and dominant frequency methods and tried to isolate the stratigraphic Q by subtracting intrinsic Q from the total attenuation. These works made clear how difficult a problem is the separation of the internal and external attenuation. Besides the fact that their effects are usually coupled, it is difficult even to get a robust estimation of their cumulative effect, since it is greatly affected by factors such as the receiver interval, interference from upgoing events, the frequency band width and the data quality.

Distinct from the above approaches, Innanen (2012) made an argument that disorder of the mechanical motions involved in a seismic wave was a common feature of both intrinsic and extrinsic Q. Treating each time trace of a VSP wave field as a sentence written in an alphabet of allowable discrete values of the displacement, the Shannon entropy (ie. the amount of information) of each trace can be calculated. The argument was that this allowed a single measure of the wave field disorder to be defined, which transfers smoothly, as time and spatial scales decrease, from characterization of multiples, to multiples beneath the resolution limit of the data, and to intrinsic Q.

1.1.3 Motivation for distinguishing different Q mechanisms

One important reason why geophysicists would like to isolate intrinsic Q from extrinsic Q is that the former is closely related to lithology and reservoir properties (permeability, gas/water saturation(Qi et al., 2017) and oil viscosity), while the latter reflects more of the underground structural change. For example, for the unconventional heavy oil reservoir, many recovery methods such as the Steam-Assisted Gravity Drainage (SAGD) involve reducing oil viscosity to let it flow spontaneously. Which calls for a good understanding of the reservoir viscosity, to better design production schemes and enhance recovery. While the viscosity in the boreholes is relatively easy to measure, additional techniques are required in the region between wells. Vasheghani and Lines (2009) showed that the viscosity of a cross-well section can be derived from the intrinsic Q by Biot-Squirt theory (Lines et al., 2013). Therefore, estimation of intrinsic Q free from effects of extrinsic Q is valuable for quantitative interpretation.

1.2 Statement of the problem

This research uses some of the same entropy ideas as Innanen (2012) to consider intrinsic and extrinsic Q in VSP data sets. Due to the unique layout of VSP data, in which wave responses are measured along the principle axis of wave propagation (i.e., the depth axis), we are able to analyze inside layers, where short-term multiples generate and scatter, and this gives the researcher a unique and detailed view of waves as they propagate.

My emphasis is on addressing the separability of intrinsic and extrinsic attenuation. To achieve the goal, a research strategy is designated. That is to view a discrete VSP data set as a 2D matrix, then calculate the Shannon entropy for each row of the matrix, corresponding to the snapshots (time traces) of the data set, and observe how entropy value evolves in time. I mainly answered the following questions in the research: does the trend of the entropy variation curve and relationship of entropy variation curves for different data sets contain sufficient information to separate stratigraphic Q from intrinsic Q? If so, to what extent does the entropy curve reflect the distinction between these types of attenuation? Are the differences qualitative only or can they be quantified? And finally, when both types of attenuation exist simultaneously in a data set, can we use its measure entropy result as an indicator of their relative strength?

1.3 Overview of chapters

This thesis is organized as follows. The theoretical foundation is given in chapter 2, where I explain the purpose and mathematical definition of Shannon entropy as well as the calculation strategy to adapt this information measure to discrete seismic records. Then I illustrate the construction of synthetic VSP models that are used to form a controlled trial aiming to observe combined and separate effects of intrinsic and extrinsic Q on Shannon entropy. In chapter 3, two entropy calculation algorithms are applied to synthetic VSP models from chapter 2 in time domain. The first algorithm, also called the first-order entropy algorithm, regard data points in a data set as independent while the second algorithm, the conditional entropy algorithm, takes correlation of two adjacent data points into consideration. After drawing some preliminary conclusions referring to entropy attributes, I investigate in chapter 4 the relationship between the measured entropy result and the relative strength of intrinsic Q and extrinsic Q when they are both active. Chapter 5 then repeats some of the experiments of chapter 3 and 4 on a field VSP data. Finally, chapter 6 includes discussions and conclusions.

1.3.1 Data used

This study involves both synthetic VSP data experiments and real VSP data experiments.

Synthetic VSPs are modelled from well log data randomly collected from a wide range of working areas, to minimize the possibility that the results are specific to one area:

(a) Two wells from Blackfoot Oilfield in Alberta, Canada. Located 15km south-east of Strathmore : 1227 and 1409 (Hoffe et al., 1998);

(b) Three wells from working area near Hussar, Alberta, Canada: 12-27-025-21, 14-27-025-21 and 14-35-025-21;

(c) Two wells from Gove and Comanche working area in Kansas, United States: Roemer-Bell No. 1-1 and Kissel A No. 1-8.

For the real data experiments, the zero-offset record of a multicomponent walkaway VSP dataset is extracted for use. CREWES participated in the data acquisition in 2011. The location and the identity of the company are not disclosed by request.

1.3.2 Software used

The synthetic VSPs are modelled in Matlab R2015a using CREWES Matlab Toolbox. The zero-offset VSP record is preprocessed in Vista 2013 provided by GEDCO/Schlumberger for free. All other calculation is realized in Matlab R2015a and Excel.

Chapter 2

THEORETICAL FOUNDATIONS

2.1 Shannon entropy

A promising way to investigate the short-term reverberations which are the source of extrinsic Q, is to measure the amount of information in the wave field. The idea is that a wave field containing complex reflecting events can be thought of as carrying a considerable amount of information, whereas a wave field excluding a complex train of reverberations might be said to have a relatively small amount of information. In information theory, measuring the amount of information of a message quantitatively has long been studied and was turned into reality by CE Shannon through "Shannon entropy" (Shannon, 2001). Thus I borrowed the concept and used it in seismology, after applying some adjustments.

A review of how Shannon entropy is developed will help in understanding the concept. In information theory, a general communication system works as in figure 2.1. According to Shannon: "The actual message is one selected from a set of possible messages. The system must be designed to operate for each possible selection, not just the one which will actually be chosen since this is unknown at the time of design." Because of this, it is important to know about the amount of information that the messages can possibly carry, to better design the system and reduce redundancy. Shannon entropy serves that purpose; It measures the amount of information contained in a message from the occurrence probabilities of elements making up the message. The less predictability the message possesses, the more information it is said to contain, and the bigger the entropy value would be.

Shannon entropy is calculated differently according to the degree of correlation allowed to approximate the information source. Take communication in English as an example. Any message will consist of some or all 26 letters from the English alphabet: a, b, c,...z. In zero-order approximation of the source (English alphabet), occurrence probabilities of all letters in this message are considered to be independent and equal, which is $\frac{1}{26}$ here. In first-order approximation of the source, the statistical knowledge of the source is incorporated. Such as in actual communication we use some letters (say a,e) more frequently than others (say x,z), so the occurrence probabilities of the former letters are set to be bigger than the latter, but are still independent. Further, there is a second-order approximation of the source. This approximation takes correlation of two successive elements into consideration, such as the likelihood of finding the letter "u" immediately after the letter "q". The occurrence probability of "u" following "q" is thus set to be bigger than others following "q". In this case, the occurrence probability of an element depends on what its immediate preceding element is, so that it is no longer independent. Correspondingly, Shannon entropies derived by using different degrees of source approximation are referred to as zero, first and second-order entropies in my research. There are higher order approximations of the source, in which the occurrence probability of an element depends on what its nth ($n \geq 3$) preceding elements are. These will not be addressed, since I have only used up to the second-order approximation.

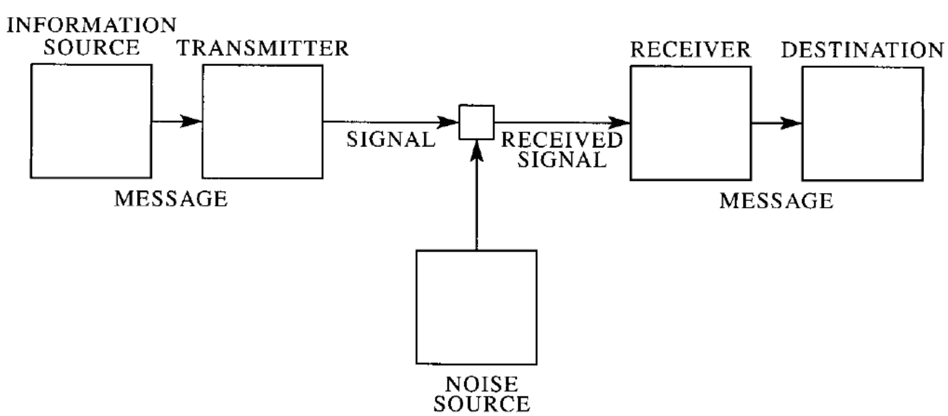

Figure 2.1: Schematic diagram of a general communication system ((Shannon, 2001)).

2.2 Defining an entropy measure for seismic records

I use the mathematical definition of the first-order entropy as an example to explain how entropy calculation in information theory can be adapted to seismic records.

2.2.1 Mathematical definition of first-order entropy

Shannon entropy was originally given in both discrete and continuous forms. The discrete form is more suitable for our research as it is intended to be applied to discrete seismic records. For an event X with possible outcomes $\{x_1, x_2, \ldots, x_n\}$ and their corresponding occurrence probabilities being $\{P(x_1), P(x_2), \ldots, P(x_n)\}$, Entropy H of event X is:

$$H(X) = -K \sum_{i=1}^{n} P(x_i) \log_b P(x_i) \tag{2.1}$$

where K is a positive constant that usually comes down to the choice of 1. And when we take the logarithm base $b = 2$, H has corresponding unit "bit".

The first-order entropy has the property of additivity. For independent events X and Y which have entropies $H(X)$ and $H(Y)$, the entropy of their joint event is:

$$H(X,Y) = H(X) + H(Y). \tag{2.2}$$

2.2.2 Adapting the entropy calculation for application to seismic records

Entropy is designed for events with uncertain outcomes, to apply it to seismic records, some adjustments have to be made. For a discrete VSP data set, assume each of its time snapshots to be a message, and data points with amplitude u_i in the snapshot can be regarded as the letters which constitute the message (figure 2.2). The entropy to be calculated is based on the probability distribution function (PDF) that reflects the chances that at any given depth the data point will have amplitude value u_i.

If each time snapshot consists of N data points (i.e. responses from N receivers), and every data point takes an amplitude value $u_i (i = 1, 2, \ldots, m)$, which represents one of m possible amplitude values, by enumerating the occurrences of a particular u_i in the snapshot as $W(u_i)$, define probability of its occurrence (Innanen, 2012) as:

$$P(u_i) = \frac{W(u_i)}{\sum_{i=1}^{m} W(u_i)}. \tag{2.3}$$

Providing a form of the probability distribution function (PDF).

In the next step, the entropy of a single data point (can be any data point in the snapshot) is calculated as in equation 2.1:

$$H' = -\sum_{i=1}^{m} P(u_i) \log_2 P(u_i). \tag{2.4}$$

The first-order entropy of a snapshot is then, making use of additivity in equation 2.2:

$$H = N * H'. \tag{2.5}$$

Equation 2.4 implies that both a greater range of possible amplitude values and a more even distribution of the amplitudes' probabilities contribute to greater entropy (figure 2.3). Overall, H should be expected to go up when the disorder of the wave field increases.

I will be observing the entropy variation with wave traveltime in the following experiments. If the disorder in a wave field increases/decreases in time, we should be able to see that on the entropy variation curve. The rate at which the entropy curve rises/drops with time may be a useful and sensitive measure of attenuating processes like absorption and stratigraphic filtering as they gradually impact the wave field during wave propagation. If we can understand how each one affects the wave field, and the entropy differently, it might even be possible to distinguish them.

2.3 Modelling of synthetic VSP

As time increases, and the seismic wave propagates through a set of layers and reverberates, H should increase. Similarly, if the wave undergoes dispersion, a growing entropy value can also be expected. What is needed in order to systematically study the influence of extrinsic and intrinsic Q on seismic wave is a VSP modelling tool by which absorption and multiples can be turned on or off at will.

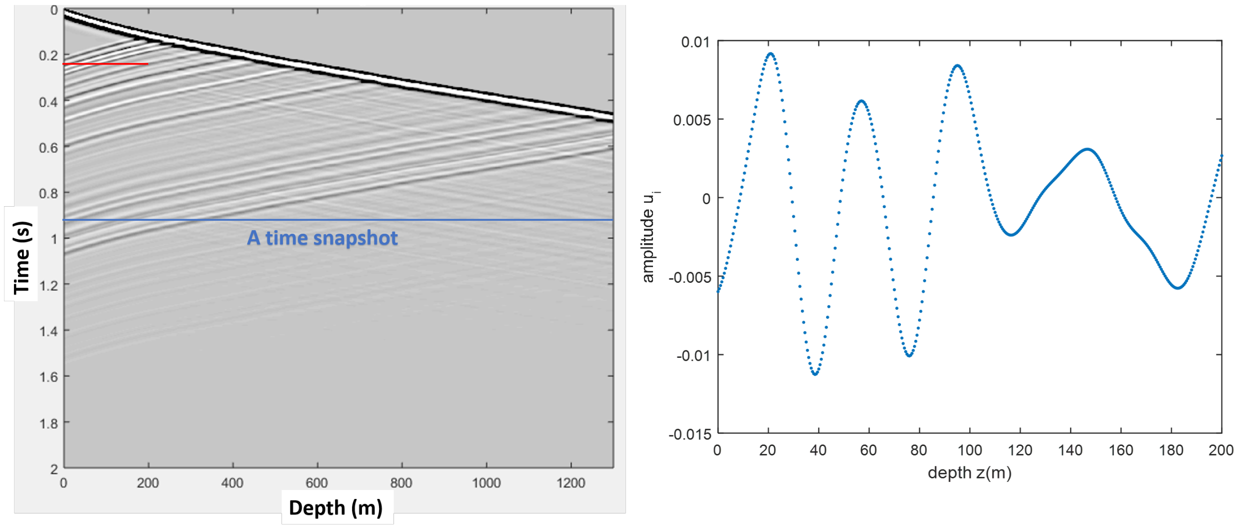

Figure 2.2: An example of a discrete VSP data set (left) and the amplitude distribution with depth zoomed on to the part covered by the red line (right). The right plot shows that the data points in the wave field are discrete.

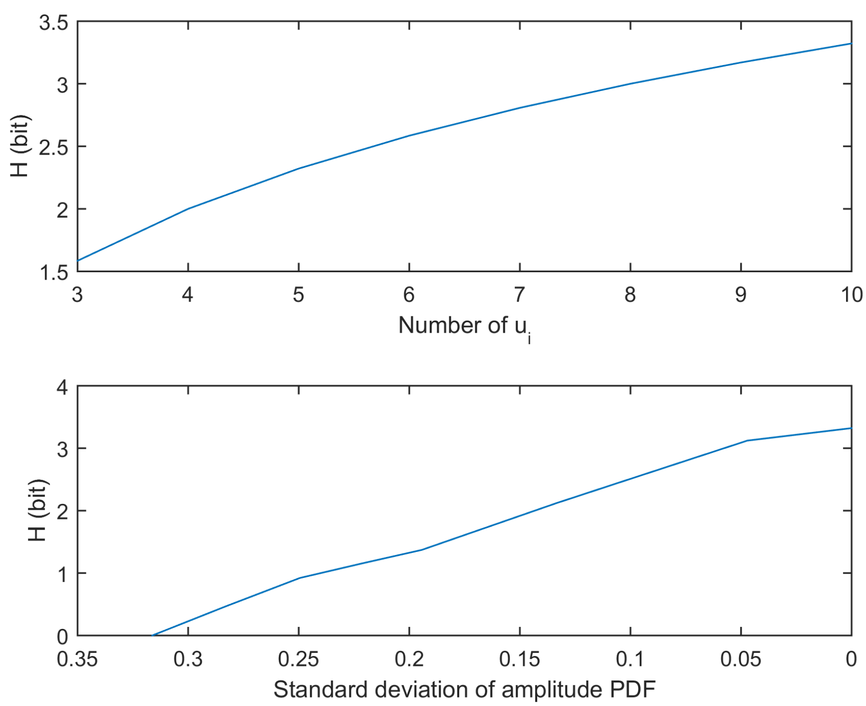

Figure 2.3: First-order entropy value of a single data point increases when there are more possible amplitude values (top) and their occurrence probabilities are more evenly distributed (bottom).

This is realized using tools from CREWES' Matlab toolbox, by which we can generate an artificial intrinsic Q distribution from P-wave velocity and density, given well logs according to empirical relationships (Margrave, 2014a):

$$Q_v(z) = Q_0 \frac{v(z) - v_1}{v_0 - v_1} + Q_1 \frac{v(z) - v_0}{v_1 - v_0} \tag{2.6}$$

and

$$Q_\rho(z) = Q_0 \frac{\rho(z) - \rho_1}{\rho_0 - \rho_1} + Q_1 \frac{\rho(z) - \rho_0}{\rho_1 - \rho_0}. \tag{2.7}$$

These equations match Q_0 with v_0 and ρ_0, Q_1 with v_1 and ρ_1, then derive the Q distribution in the whole depth range based on these two points. The values v_0, ρ_0, v_1 and ρ_1 are all available from standard well logs. The final Q model is derived according to the following equation to combine the estimations.

$$\frac{1}{Q(z)} = \frac{1}{2}\left(\frac{1}{Q_v(z)} + \frac{1}{Q_\rho(z)}\right). \tag{2.8}$$

Once a defensible Q model is determined, synthetic VSPs are modelled by a propagator matrix method (Margrave and Daley, 2014b). The reason the propagator matrix approach is chosen is that with it one can conveniently turn on and off internal multiples, surface multiples, transmission loss and absorption in the finalized VSP data set. This way, the influence of these elements on the entropy, alone or together, can be studied.

Chapter 3

TIME DOMAIN INFORMATION MEASURES

3.1 Chapter overview

The time domain information measure consists of two parts, one involving a first-order entropy algorithm to compute the first-order entropy of the VSP data and also a conditional entropy algorithm to compute the second-order entropy of the VSP data. The first-order entropy study uses the measure of entropy described in last chapter, which is not sensitive to correlations between nearby wave field values. After that, a conditional entropy algorithm utilizing conditional amplitude probabilities is constructed, allowing correlations between two adjacent data points to be included.

In the calculation process there are some points to emphasize:

(1) Both the seismic data and the entropy calculation are discrete, which means we have to define and use amplitude bins to classify data points. A proper choice of amplitude binning is crucial, to ensure that diverse subsurface events (direct arrival, primaries, internal multiples, etc.) can be distinguished and will have the appropriate effect on the computed entropy;

(2) A range for possible amplitude values needs to be determined for amplitude PDF calculation.

3.2 Data set

Well log data randomly collected from a wide range of working areas were used in the experiment, to minimize the possibility that the results are particular to one area:

(a) Two well logs from Blackfoot Oilfield in Alberta, Canada. Located 15km south-east of Strathmore (figure 3.1): 1227 and 1409 (Hoffe et al., 1998);

(b) Three well logs from working area near Hussar, Alberta, Canada (figure 3.2): 12-27-025-21, 14-27-025-21 and 14-35-025-21;

(c) Two well logs from Gove and Comanche working area in Kansas, United States: Roemer-Bell No. 1-1 and Kissel A No. 1-8 (figure 3.3).

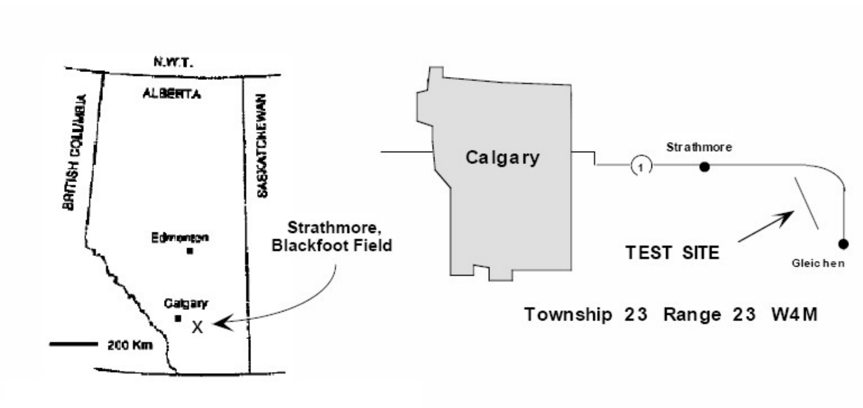

Figure 3.1: Location of the Blackfoot Oilfield.

3.3 The first-order entropy algorithm

3.3.1 Calculation strategy

For both algorithms, a controlled trial of entropy calculation was carried out, composed of four distinct synthetic zero-offset VSP data sets built from well logs described above. The VSP data sets contain respectively: a) primaries; b) primaries with internal multiples; c) primaries with absorption and d) primaries with both absorption and internal multiples. Which represent, correspondingly, earth models of the following type: a) a non-absorptive slab; b) a non-absorptive finely layered sequence c) an absorptive slab and d) an absorptive finely layered sequence. Note that the surface-related multiples are not modelled in any of the data sets as they will scatter the wave amplitudes and increase the disorder in the wave field in the similar way as internal multiples, which makes them an interference for our research.

Figure 3.2: Location of Hussar wells.

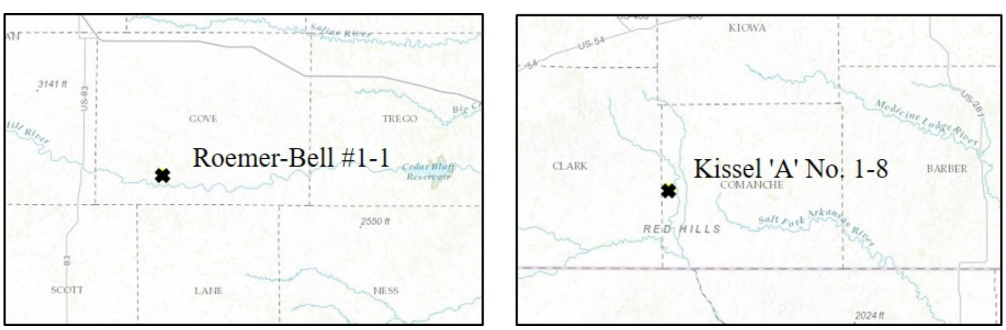

Figure 3.3: Location of Kansas well Roemer-Bell No. 1-1 randomly and well Kissel A No. 1-8.

The complete time domain information measure is conducted in the following steps:

(1) Create a "fake Q" model from the well log;

(2) Generate four synthetic VSP data sets for the controlled trial using the propagator matrix method;

(3) Choose a proper amplitude bin size according to source wavelet and the seismic record;

(4) Calculate an amplitude PDF for every time snapshot of all VSP data sets;

(5) Calculate entropy for every time snapshot of all VSP data sets using the amplitude PDFs.

3.3.2 Choice of bin size

A proper choice of amplitude bin size is crucial for the entropy calculation because it determines how distinct the event classification will be, and this impacts the final entropy behavior. It needs to be sensitive enough to the energy scale difference between direct arrival and primaries, between primaries and multiples and between noise and weak signals, so that their impact on entropy curves can be properly distinguished.

Taking well 1227 from Blackfoot oilfield as an example, figure 3.4 presents its forward modelling result of step (2), and figure 3.5 shows the minimum phase source wavelet with main frequency 30hz used throughout the modelling process. It was observed that the source wavelet has a maximum absolute amplitude of approximately 0.13 and data points in the figure 3.1 wave fields have absolute amplitudes ranging from 0 to 0.1. Thus I empirically decided that the amplitude bin size be smaller than 0.1 to guarantee a good resolution. As a result, three bin sizes 0.01, 0.001 and 0.0001 were chosen and tested.

It can be difficult to determine which choice of bin size is more appropriate by simply observing the amplitude values in the wave field. Instead, I devised a criterion: the proper bin size should be able to distinguish the upgoing events in the presence of the much stronger downgoing events' energy. Downgoing waves in real VSP seismic records have much stronger energy than upgoing events because of the cumulative effects of wave attenuation like geometrical spreading, absorption and transmission loss with increasing propagating time; so the upgoing energy in a VSP record is usually overwhelmed by the downgoing energy. Yet for our study of stratigraphic filtering, upgoing energy is too important to be neglected, as it contains information about all kinds of reflections. Therefore, the amplitude bin chosen should be able to distinguish upgoing events to ensure they will affect entropy properly.

The next question is how to decide whether the upgoing events are, in fact, detected? In the forward modelling process, we lose some of the downgoing events by turning off the surface multiples. Accordingly, I found, in all modelled VSP data sets, there are more upgoing events than downgoing events (among those which have no more than three bounces. Events that have more than three bounces are considered to have negligible energy.) (see appendix B). From information theory perspective, this means the upgoing wave field is more disorderly than the downgoing wave field regardless of their energy levels. So that the former is expected to contribute to a slightly larger entropy value than the latter when determining proper bin sizes.

Figure 3.6 displays the entropy evolution with time for up and downgoing wave fields associated with the figure 3.4 data sets. Each subplot is composed of four panels, corresponding to four VSP data sets. The bin sizes used to derive (a), (b) and (c) are respectively 0.01, 0.001 and 0.0001. In subplot (a), entropy of the downgoing wave field exceeds entropy of the upgoing wave field when neither absorption nor internal multiples exist (upper left panel), which indicates that bin size 0.01 is unsuitable. In subplot (c), entropy of downgoing wave field exceeds entropy of upgoing wave field so greatly that we can hardly distinguish between the four panels that reflect diverse subsurface features. It is likely that the calculation errors (eg. when all signals have passed, the data sets are not filled by exact 0s but numbers that are very close to 0) are misinterpreted as signals by the amplitude bin with size 0.0001. Subplot (b), on the other hand, gives the relatively satisfactory result that upgoing and downgoing wave fields' entropies are comparable, and they possess enough sensitivity to the different subsurface features between four panels. Based on the tests, therefore, bin size 0.001 appears to be the most appropriate choice for the research.

3.3.3 Blackfoot well 1227 results

I found that the trends and relative relationships of entropy variation curves of all the tested wells are similar, suggesting that the information measure is robust. Consequently, the general features of the results can be outlined by focusing on a particular well. To exemplify the results I consider the Blackfoot well 1227. Table 1 contains some key parameters that are used in the experiment.

A "fake Q" distribution is created for Blackfoot 1227 and is plotted in figure 3.7. The four VSP data sets for the controlled trial are then modelled and shown in figure 3.4. Based on equation 2.3, PDFs representing the probability of a particular amplitude value's occurrence in a snapshot of the VSP wave fields are derived and shown in figure 3.8. Then, using equation 2.4 and 2.5, entropy H for each snapshot of the wave fields is calculated. Finally, the entropy variation with time results of all wave fields are shown in figure 3.9.

Table 3.1: Key parameters used in modelling synthetic VSP data

Q		Geophone				Amplitude bin size
Minimum Q	Maximun Q	Interval (m)	Depth Range (m)	Dominant f of wavelet (Hz)	Maximum traveltime (s)	
20	220	0.5	0-1300	30	2.0	0.001

The amplitude PDFs in figure 3.8 allow some qualitative interpretations to be made. Each row in the subplot stands for the amplitude PDF computed at a certain time snapshot; scanning the plots vertically permits us to discuss the variation of PDF with time in the wave field. According to the definition of the amplitude PDF, the more spread the PDFs in a subplot are, vertically or horizontally, the more severely the amplitude is scattered in the corresponding wave field.

The most noticeable fact is that, after a certain time, all PDFs become completely centralized. This represents a baseline, or zero state, after all signal information has passed; noise and artifacts fill one bin of the histograms here.

Comparison among subplots (a), (b), (c) and (d) allows some preliminary conclusions to be

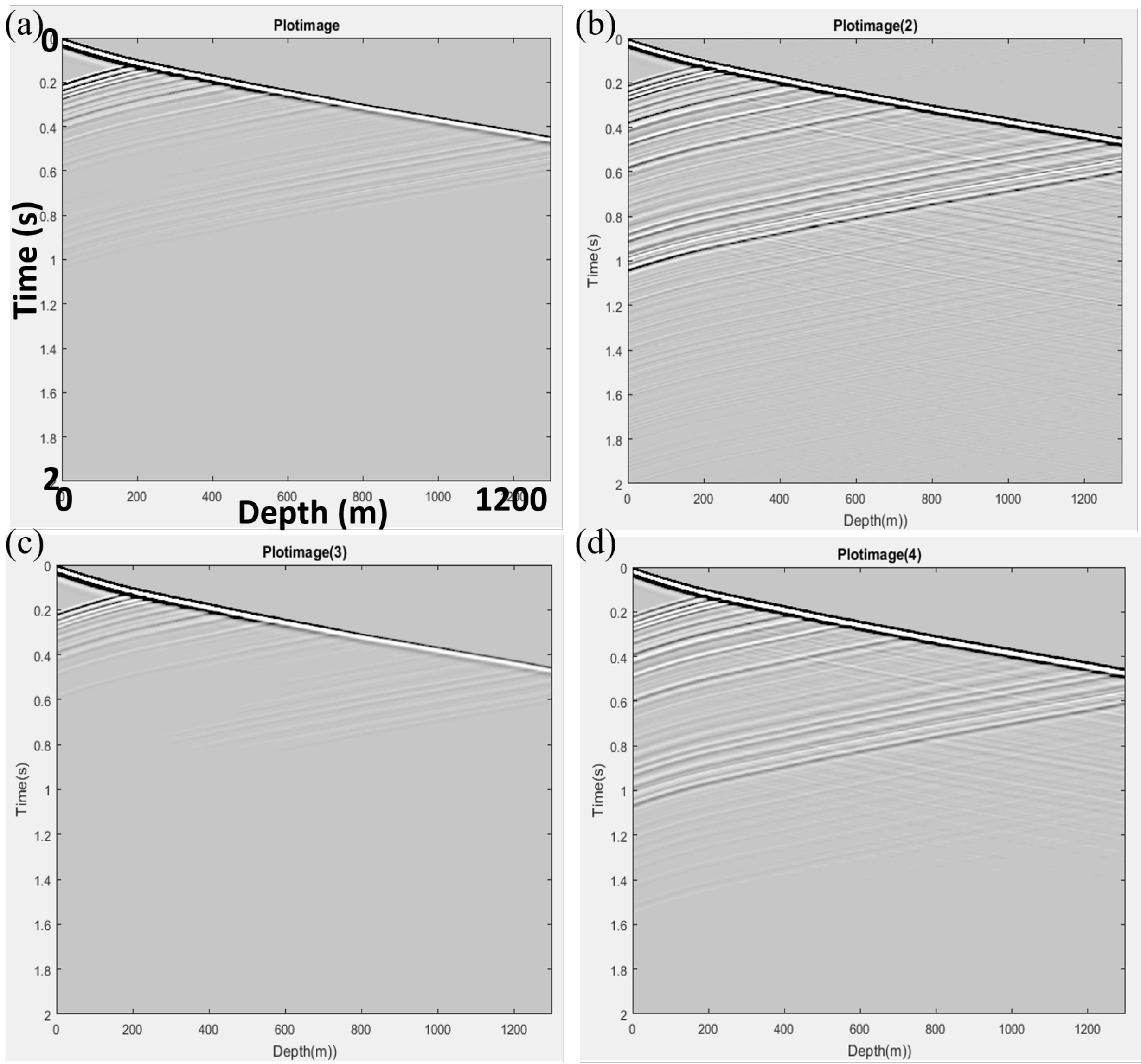

Figure 3.4: Synthetic VSP data sets modelled from well Blackfoot 1227 representing the following subsurface features: a) a non-absorptive slab; b) a non-absorptive finely layered sequence c) an absorptive slab and d) an absorptive finely layered sequence.

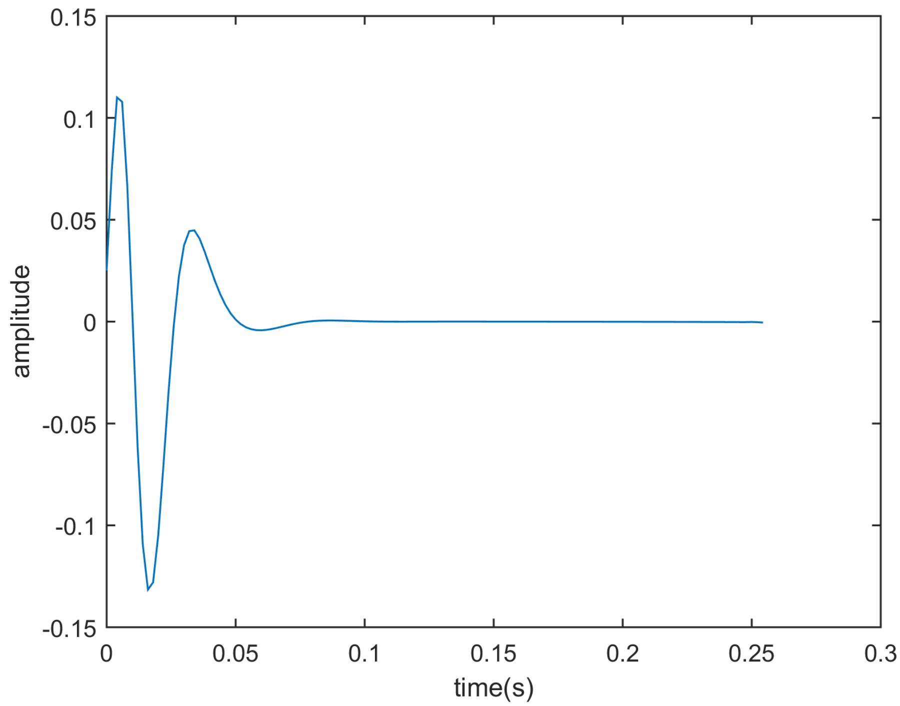

Figure 3.5: The minimum phase 30hz source wavelet used for forward modelling.

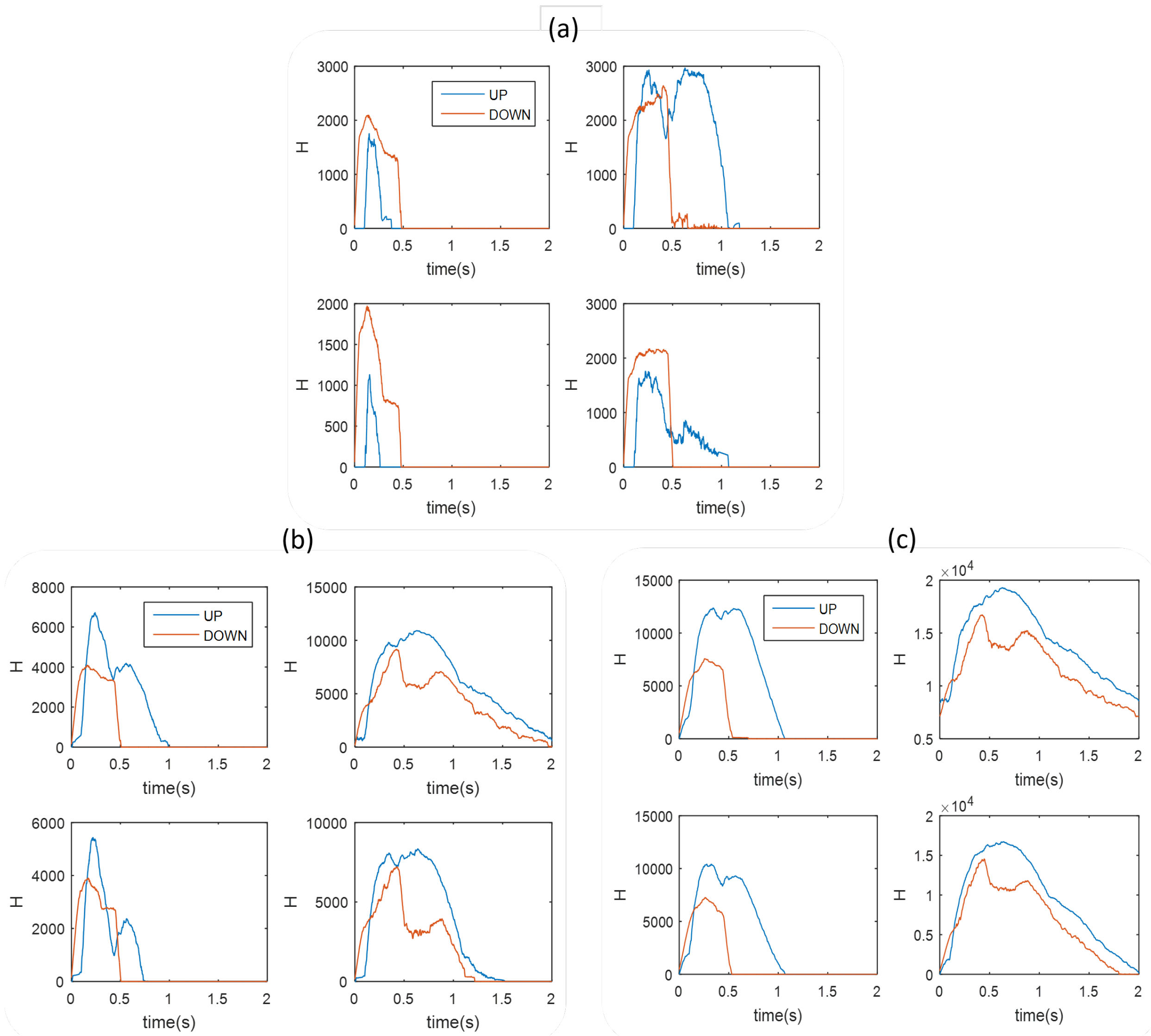

Figure 3.6: The entropy variations with time for up and downgoing wave fields in figure 3.4 data sets using respectively amplitude bin size (a) 0.01 (b) 0.001 (c) 0.0001.

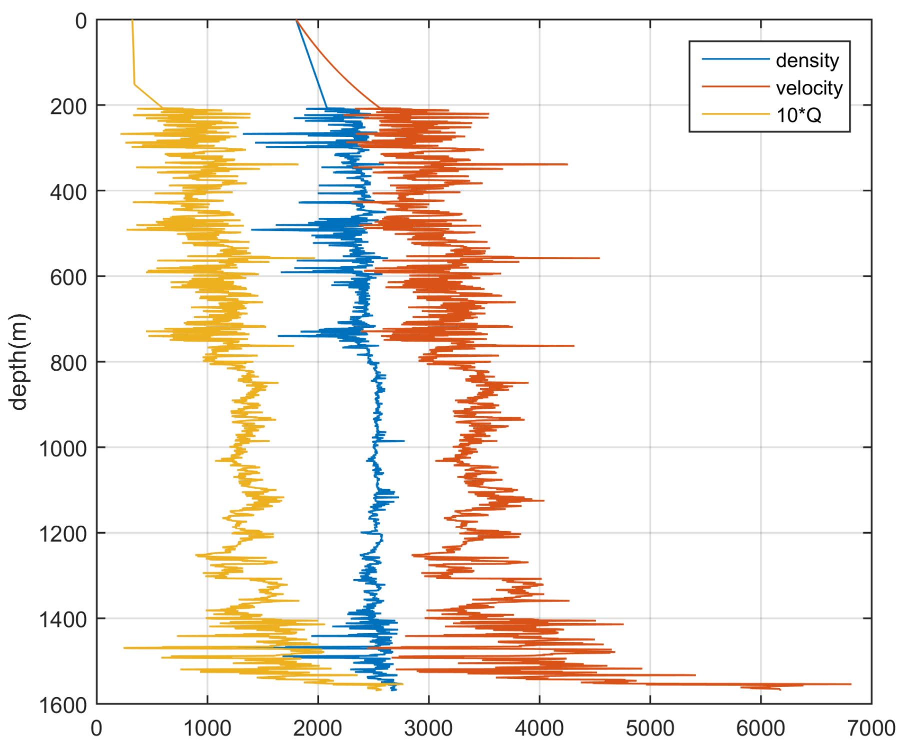

Figure 3.7: Empirically simulated Q distribution, sonic (P-velocity) log and density log of well Blackfoot 1227.

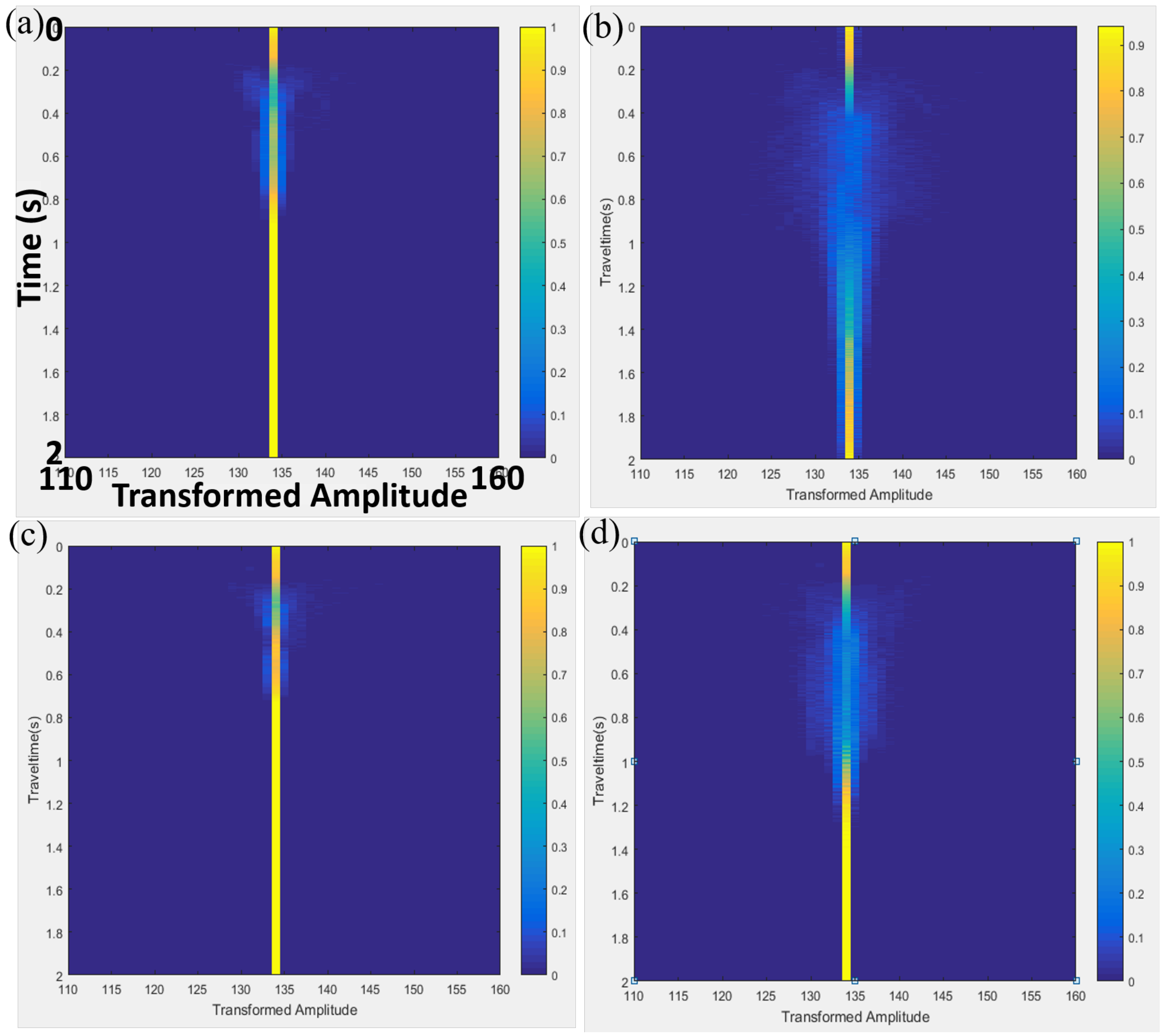

Figure 3.8: The independent amplitude PDFs derived respectively from synthetic VSP data sets in figure 3.4.

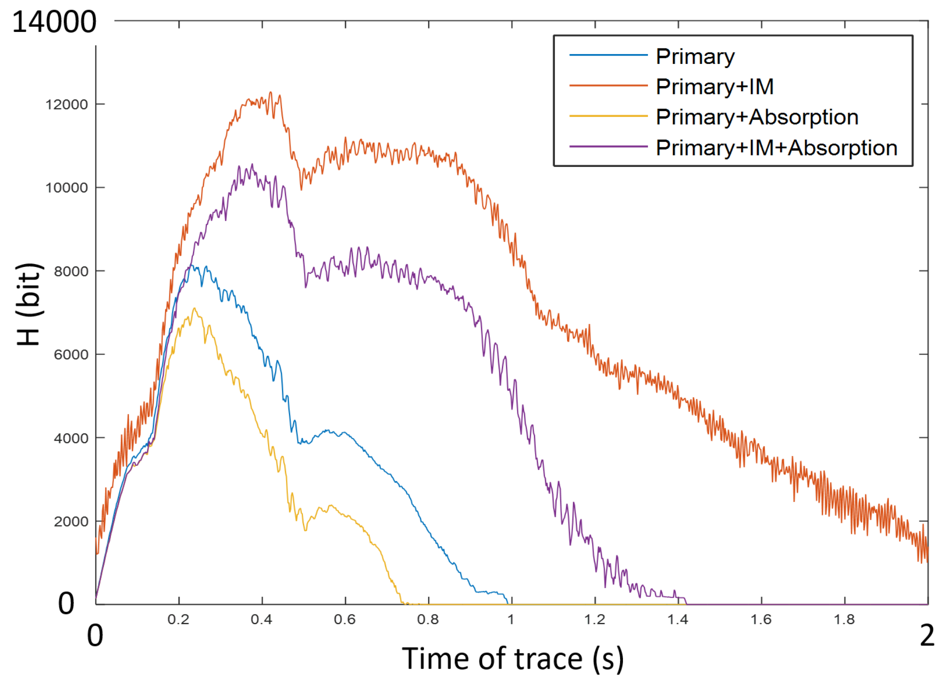

Figure 3.9: The first-order entropy variation result of synthetic VSP data sets in figure 3.4.

drawn:

(1) Comparing (b) to (a), existence of internal multiples extends the amplitude scattering vertically to later arrival times and horizontally to wider range, such that the disorder in the wave field is increased overall;

(2) Comparing (c) to (a), absorption impacts amplitude scattering in exactly the opposite way: the scattering effect shrinks horizontally to a smaller range and vertically to earlier arrival times, which represents a decrease of the disorder in the wave field;

(3) Lastly, with internal multiples and absorption acting simultaneously in case (d), amplitude scattering lies in a status between that of (b) and (c) where internal multiples and absorption act separately: it extends vertically to a later arrival time than (c) while the amplitude scattering range shrinks horizontally to a smaller value than (b).

It appears that the effects of internal multiples and absorption on the amplitude PDFs counteract each other. Why this happens needs further investigation, but it at least suggests that the information measure may be sensitive enough to distinguish between the two attenuation mechanisms. This leads us to analysis of figure 3.9.

In figure 3.9, for all situations, entropy increases with time at starting portion, reflecting the growing disorder with time of the wave fields. However, the increase is different for each of the four cases. Derived from cases excluding internal multiples, the yellow and blue curves have smaller peak entropy values than red and purple ones. They peak at between 0.2s and 0.3s, which can be regarded as a direct response to the primaries generated from a cyclic layered region, in other words, a region where velocity and density change rapidly between large and small values over a small depth interval: 200m-300m (see figure 3.7). On the other hand, cases including internal multiples (purple and red curves) contribute to larger peak entropy values at a later time around 0.4s. From the delayed peak time I infer that the first-order multiples from the same cyclic layered region are making the greatest contribution to the rise of entropy. Furthermore, entropies calculated from cases containing absorption exhibit smaller peaks than those which do not, as seen by comparing purple and yellow curves to the red and blue ones respectively. Overall, the most disordered PDFs (figure 3.8 (b)) contribute to the largest entropy (red curve) and vice versa (yellow curve).

No analysis for the decreasing portions of the entropy curves has been made, since I was able to prove that the decrease is more of an artifact of the discrete entropy algorithm. Intuitively, one would expect that the entropy of an isolated wave field remains constant or increases, never decreases. Why entropy decreases after a certain point in time is explained as follows. In figure 3.10, subplots in the left column imitate the possible amplitude distribution of a VSP snapshot. In the case that the original amplitudes are attenuated by 90% (from (a) to (b)) while the bin size stays fixed as 1, there will be an observable change in the corresponding PDF. When data points assume smaller values, amplitudes are more coarsely sampled by the constant bin size, leading to a narrower, steeper PDF, and hence to a smaller entropy value. In other words, entropy decrease is a consequence of data amplitude range diminishing relative to bin size, not of the decrease in wave field disorder.

During wave propagation, internal multiples scatter waves and distribute wave energy into smaller packets (eg. incident wave generates reflected wave and transmitted wave at an interface, both of which have smaller amplitudes than the incident wave), and absorption transforms wave energy into heat. Both mechanisms gradually attenuate the amplitudes and make our measure of entropy decrease after a certain time. Nevertheless, internal multiples boost the amplitude scattering in the field while absorption does the opposite (figure 3.8), so they have different effects on entropy.

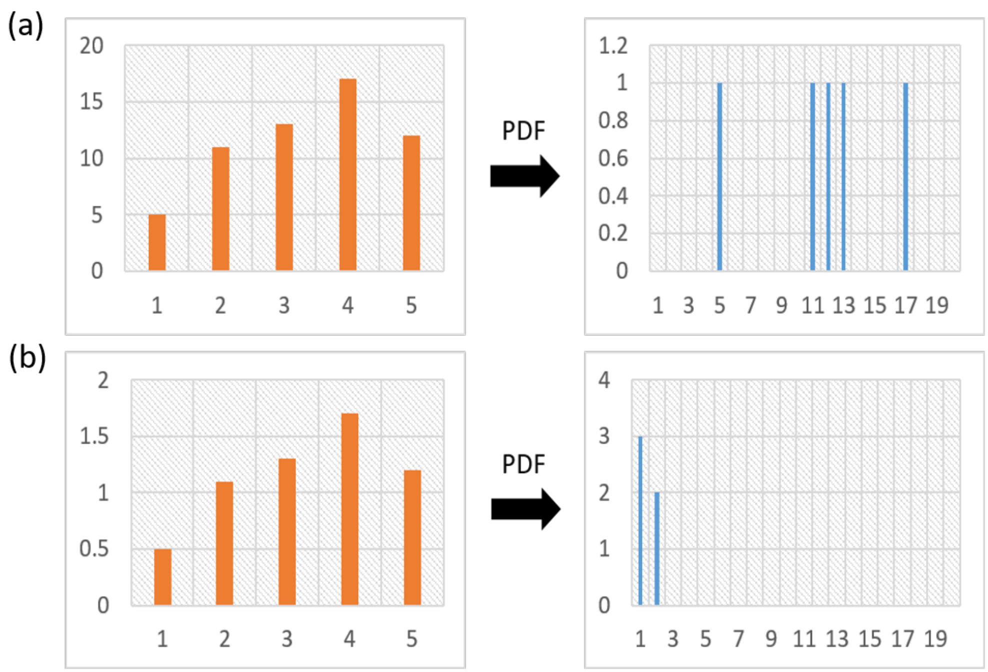

Figure 3.10: Simulation of amplitude distribution in a VSP time snapshot before (a) and after (b) attenuation and their corresponding amplitude PDFs.

3.3.4 Seven-well comparison

The first-order entropy variation results for seven wells are calculated and shown in figure 3.11, followed by table 3.2 listing the peak values of all curves for the convenience of comparison. Discrepancies exist among results of different wells due to the diverse geological condition surrounding the well positions, nevertheless all curves share some common features: all entropies increase with wave propagation in early time range 0-0.5s. Also, the peak values of four entropy curves for any well are ranked from high to low as: case (b), the one involves solely internal multiples; cases (d) or (a), those involve both internal multiples and absorption or involve neither internal multiples nor absorption, and, case (c) which involves solely absorption. The first-order entropy algorithm seems to be robust across at least three randomly selected analysis areas, and the the analysis is similar for every well.

Table 3.2: Peak values of the first-order entropy variation results

	A	B	C	D
Roemer Bell No. 1-1	8802.2	14532	7855.4	12903
Kissel A No. 1-8	11199	13837	9881.3	12128
Blackfoot 1227	8170	12297	7079.3	10528
Blackfoot 1409	13138	13816	11177	11926
Hussar 12-27-25-21	8170.3	12297	7114	10656
Hussar 14-27-25-21	7809.5	12270	6778.5	10546
Hussar 14-35-25-21	7648.2	11933	6475.2	10413

[1] Straight line marks the maximum among horizontal four values, wave line marks the minimum

3.4 The conditional entropy algorithm

Analysis regarding the first-order entropy algorithm suggests that a sensitive information theory based analysis could uncover distinctions between intrinsic and extrinsic attenuation. However, the first-order approximation of the wave field data does not take correlations between nearby data points into account, and it is plausible that involving these correlations will help emphasize differences between extrinsic and intrinsic Q. Empirically we know that for a bandlimited, continuous seismic waveform, if at one time amplitude has a particular value, amplitude at its neighboring time is not arbitrary, but is likely to fall near this value. In this part I will demonstrate the usage of this correlation in analyzing seismic data.

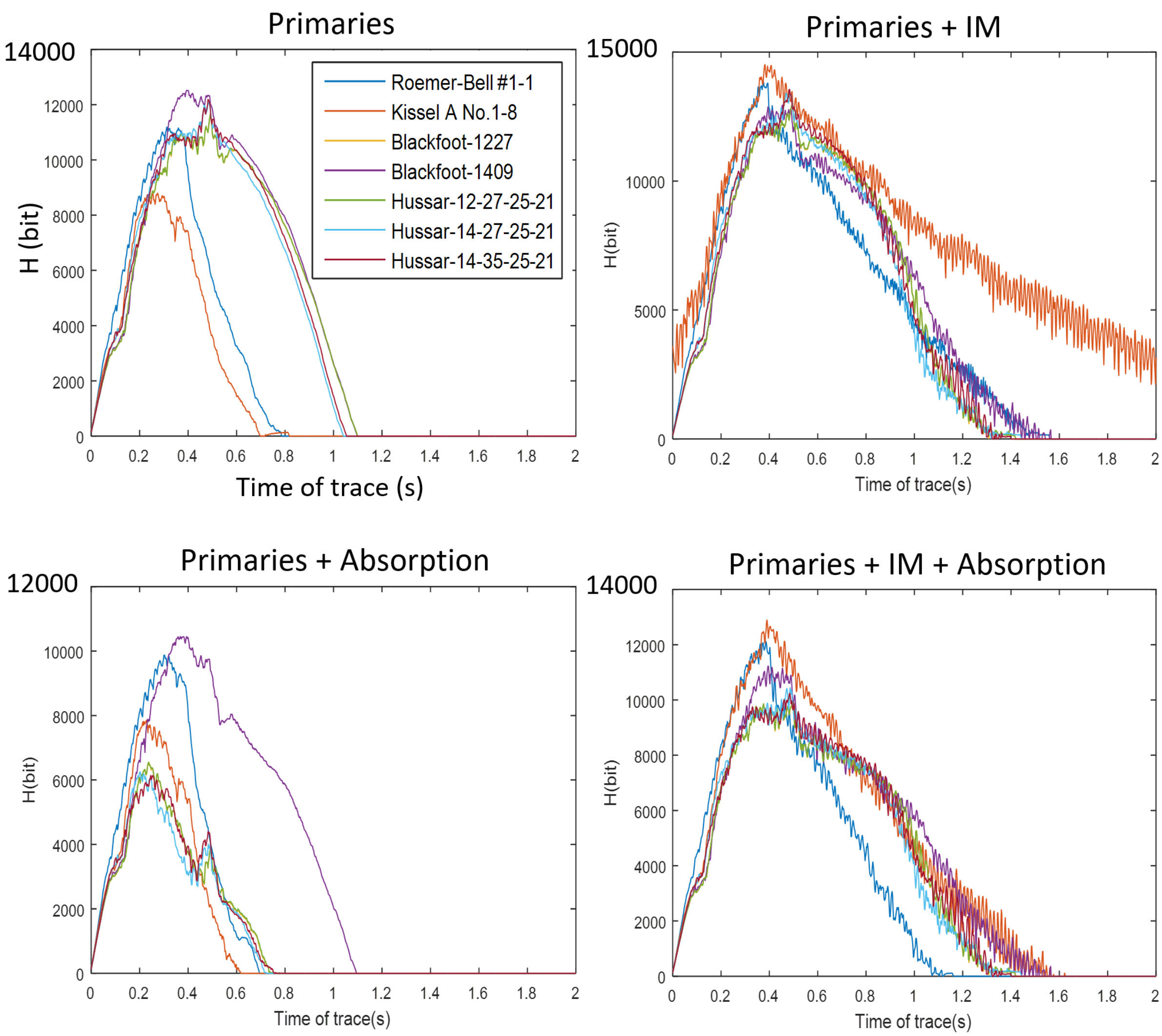

Figure 3.11: The first-order entropy variation results of synthetic VSP data sets built separately from seven wells representing the following subsurface features: a) a non-absorptive slab; b) a non-absorptive finely layered sequence c) an absorptive slab and d) an absorptive finely layered sequence.

I used a second-order approximation of the wave field and from that developed a conditional entropy algorithm, in which the probability of selecting a value at one data point is considered to be determined by the value of its immediately preceding data point in time. Entropy derived this way is called second-order entropy. The conditional algorithm was applied to all wells. In the following section, I still use well Blackfoot 1227 as a representative.

3.4.1 Calculation strategy

To determine the correlation of amplitude values, I chose a particular value as prerequisite and computed the occurrence frequencies of all possible values at its succeeding time position in a whole data set range. The occurrence probabilities derived this way is called conditional probabilities in statistics. The conditional PDFs computed for VSP data sets in figure 3.4 is displayed in figure 3.12. Probabilities for all data sets distribute along diagonals, indicating all subsequent amplitude values correlate strongly with their preceding values, which one might intuitively expect.

If the independent PDF of an event X is $P(x_i)$ $(i = 1,2,\ldots,n_1)$, and the conditional PDF of event Y happening right after it is $P(y_j|x_i)$ $(j = 1,2,\ldots n_2)$, the second-order entropy is computed by (Shannon, 2001):

$$H(Y|X) = \sum_{x_i} P(x_i) H(Y|X = x_i) = -\sum_{x_i} P(x_i) \sum_{y_i} P(y_i|x_i) \log P(y_i|x_i). \qquad (3.1)$$

$H(Y|X = x_i)$ represents the conditional entropy of Y with prerequisite X having a certain outcome x_i. In this experiment, X stands for the starting amplitude U_0, and Y stands for its succeeding amplitude U_i in figure 3.12. With the conditional entropy $H(Y|X)$ of Y and the first-order entropy $H(X)$ of X, entropy of the joint event of X and Y can be derived by:

$$H(X,Y) = H(Y|X) + H(X). \qquad (3.2)$$

The research strategy was still investigating how entropy evolves in time, which requires that an entropy value be computed for every time snapshot. To incorporate the amplitude correlations displayed in figure 3.12, I determined the first-order entropy for the first point in the snapshot

H_1 according to equation 2.4, using the independent amplitude PDFs in figure 3.8. Then, with equation 3.1, the independent PDFs of the leading point and conditional PDFs of the following point were combined to give entropy of the second point in condition of the first point taking particular amplitudes, being referred to as $H_{2|1}$. Summation of H_1 and $H_{2|1}$ gave $H_{1,2}$— entropy of the first two points taking particular amplitudes simultaneously. Following this idea, entropy of the whole snapshot was suppose to be $H_{1,2,...,N} = H_1 + H_{2|1} + H_{3|1,2} + \ldots + H_{N|1,2,...,N-1}$. However, first, $H_{1,2,...,N}$ is not second-order but Nth-order, which is not in accordance with my intention of using second-order source approximation; second, calculating the Nth-order probabilities when N is big can hardly be achieved in Matlab because it requires a tremendous amount of time and storage. Thus, I made a compromise and assumed $H_{3|1,2}, H_{4|1,2,3}, \ldots, H_{N|1,2,...,N-1}$ to be all equal to $H_{2|1}$, which made the entropy of a snapshot

$$H = H_1 + (N-1)H_{2|1}. \tag{3.3}$$

3.4.2 Blackfoot well 1227 results

The following observations are made regarding figure 3.13, in contrast to the results of the first-order entropy algorithm (figure 3.9):

(1) The magnitude: the magnitude of the entropy values is greatly reduced due to the use of conditional probabilities by which highly impossible amplitudes values are eliminated;

(2) The trend: Focusing on time range 0-0.5s where events are better resolved by the amplitude bin, the entropy curve is dominated by a steep decline, after an initial brief rise;

(3) The interrelation: peaks of entropy curves for cases including internal multiples (red and purple curves) lie generally beneath those for cases excluding internal multiples (yellow and blue curves), and the involvement of absorption in wave fields contributes to entropy curves with relatively larger peak values (yellow and purple curves in contrast to the blue and red ones respectively).

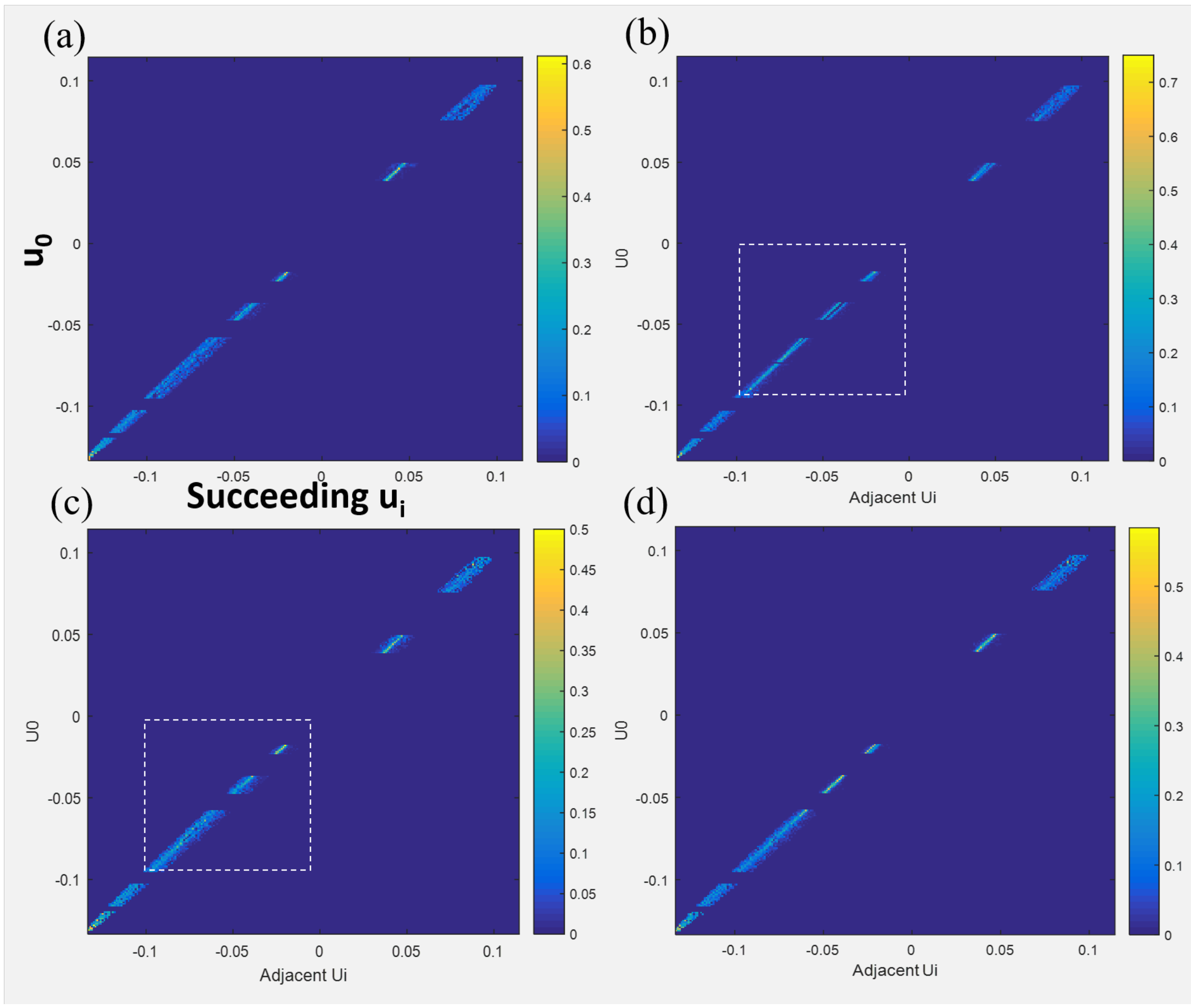

Figure 3.12: Conditional PDFs of amplitude U_1 in condition of its leading points in time having amplitude U_0 from synthetic VSP data sets of figure 3.4 (several points around zero are muted). The white squares direct attention to regions with apparent distinguishing features.

Some of the above observations are unexpected because they contradict some conclusions that were drawn in the first-order entropy algorithm. One confirmation is that the involvement of data point correlations has complicated the problem. The final analysis should await the results from other six wells, however.

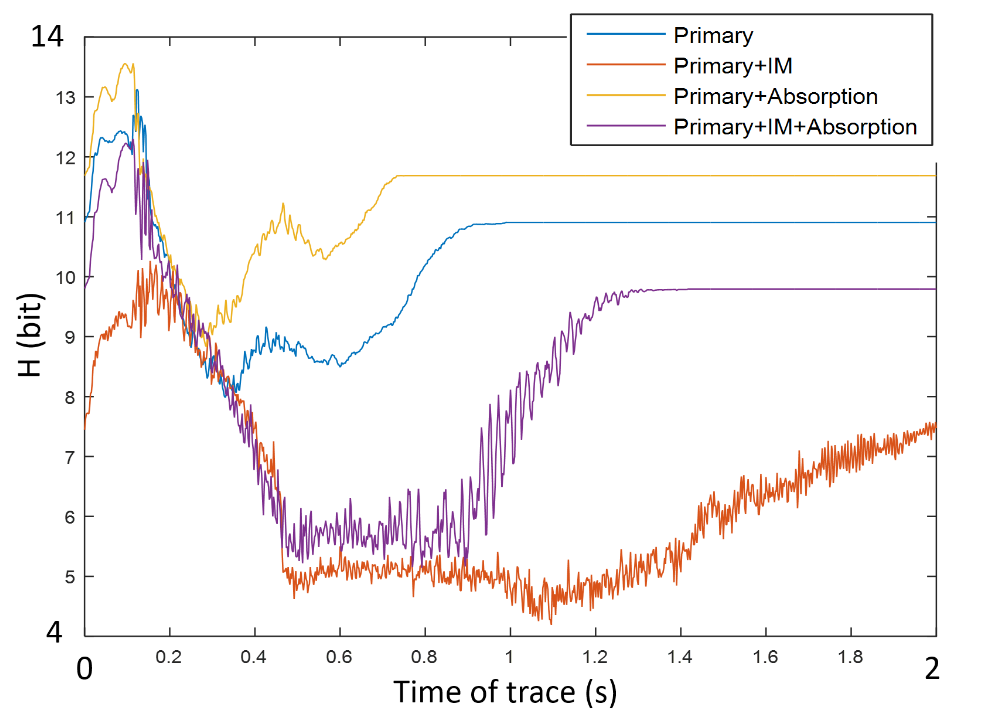

Figure 3.13: The second-order entropy variation result of synthetic VSP data sets in figure 3.4.

3.4.3 Seven-well comparison

Figure 3.14 shows the comparison of conditional entropy measures of all wells. Table 3.3 lists the peak values of all entropy curves. On one hand, figure 3.14 appears to show some common features among different entropy curves, such as that they all have small magnitudes and similar trends—they generally decline after a short-period rise. On the other hand, numbers in the table reveal that results from other six wells do not share all the characteristics of Blackfoot 1227 entropy curves. The peak values are irregularly ordered from high to low, which obscures the manner in which intrinsic and extrinsic Q affect entropy in the new algorithm.

Nevertheless, when zooming on the rising portion of entropy curves which lies in time range 0-0.15s (figure 3.15), entropy curves for all wells show consistency in their correlations: entropy of case (c) including only absorption has the largest value, followed by entropy of case (d), including both absorption and internal multiples, and entropy of case (a) including neither absorption nor internal multiples; case (b) which includes only internal multiples has the smallest entropy value.

An explanation for the above behavior can be given intuitively. Each seismic event in the wave field represents an amplitude sequence. Since we are reducing the uncertainty of the amplitude values by making use of the natural extent of the waveform in the conditional entropy algorithm, more events in the field will increasingly constrain subsequent points in these sequences. The effect of this is to narrow the amplitude PDF, which leads to a smaller entropy. Internal multiples, as an exterior factor, increases the number of events in the wave field while absorption does the opposite by attenuating amplitudes and making seismic events lose relative to the amplitude bin, then being undistinguishable. Proof can be found in the tighter PDF in squared region of figure 3.12 (b) than (c).

Table 3.3: Peak values of conditional entropy variation results

	A	B	C	D
Roemer Bell No. 1-1	13.7	8.6	13.25	12.3
Kissel A No. 1-8	14.86	15.03	14.95	14.24
Blackfoot 1227	13.12	10.26	13.54	12.23
Blackfoot 1409	15.54	14.32	13.05	12.39
Hussar 12-27-25-21	13.12	10.26	13.53	12.17
Hussar 14-27-25-21	13.75	15.1	13.83	12.65
Hussar 14-35-25-21	13.82	15.52	13.79	12.76

3.5 Chapter summary

Two time-domain entropy algorithms yield very different results, but analysis suggests they can both be reasonable, depending upon the point of view. One measure of entropy is positively related

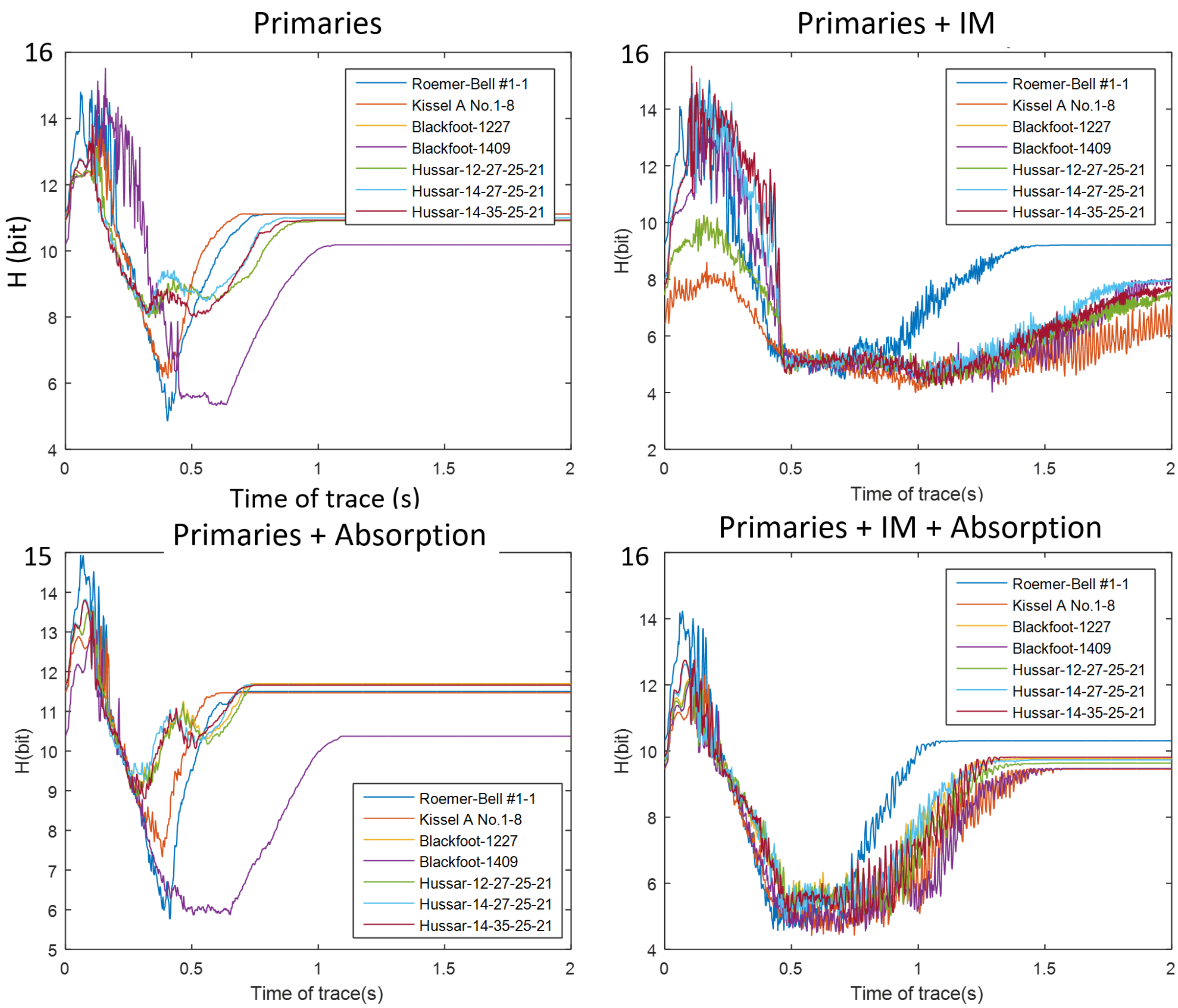

Figure 3.14: The second-order entropy variation result of synthetic VSP data sets built separately from seven wells representing the following subsurface features: a) a non-absorptive slab; b) a non-absorptive finely layered sequence c) an absorptive slab and d) an absorptive finely layered sequence.

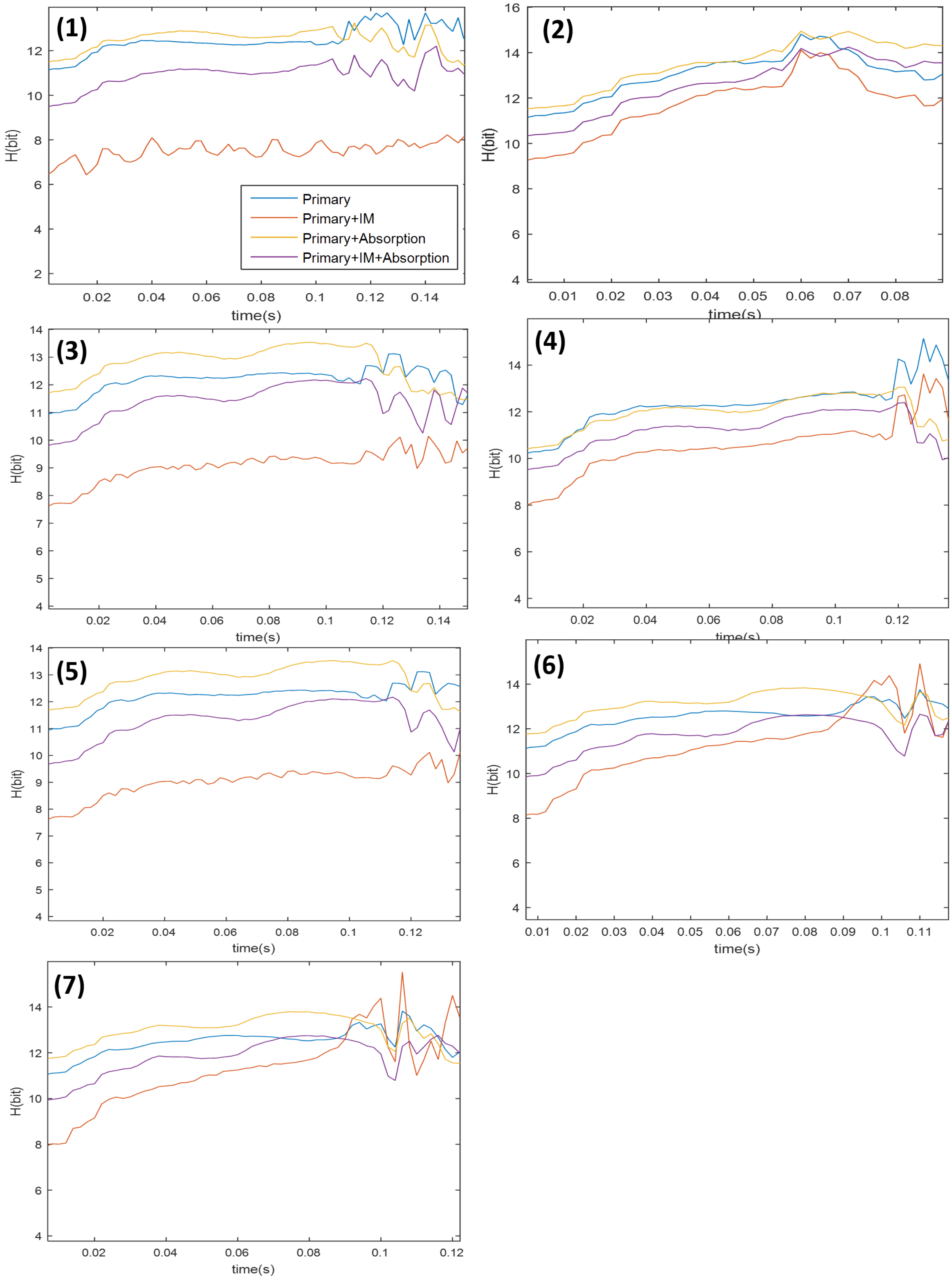

Figure 3.15: Results for different wells in figure 3.14 zooming on early times. (1) Roemer Bell No.1-1; (2) Kissel A No.1-8; (3) Blackfoot 1227; (4) Blackfoot 1409; (5) Hussar 12-27-25-21; (6) Hussar 14-27-25-21; (7) Hussar 14-35-25-21.

to the change of disorder in the wave field as waves propagate, the other is bounded by data points' increasing correlations as a consequence of an increasing number of events. It is encouraging to see that, no matter in which algorithm, intrinsic Q and extrinsic Q always influence entropy in the opposite sense. Although the entropy behaviour depends closely on the amplitude bin resolution, it does not mean we can not make use of this attribute to let it assist in distinguishing the different attenuation mechanisms.

From the perspective of using information measure to recognize and separate intrinsic and extrinsic Q in the wave field, the first-order entropy algorithm is preferable to the conditional entropy algorithm. While both of them are sensitive to the distinction between different Q, the former presents it in a more straightforward manner. There is also promise in using the information measure to evaluate the relative strength of stratigraphic Q and absorptive Q in a scenario when their effects on the seismic wave are inseparable. This can be possibly achieved by comparing the entropy curve of case (d)—wave field includes both absorption and internal multiples, with the entropy curve of case (a)—wave field includes neither absorption nor internal multiples.

Chapter 4

THE INFORMATION MEASURE WHEN BOTH INTRINSIC AND EXTRINSIC Q ARE ACTIVE

4.1 Chapter overview

It is shown in last chapter that the time domain entropy responds differently in the presence of intrinsic Q and extrinsic Q in the wave field, which suggests that the information measure may be used to distinguish them. I conjectured that comparing the entropy variation curves of two cases in the controlled trial: case (a) and case (d), will reveal information regarding the relative strength of two attenuation mechanisms when they act simultaneously on seismic waves.

This chapter demonstrates how I attempted to verify the conjecture. A new experiment was designed utilizing synthetic data and entropy results from all seven wells. The previous chapter focused mostly on entropy analysis of wave fields generated by either an absorptive slab (case (c)) or a non-absorptive finely layered sequence (case (b)). This chapter, however, pays attention to the entropy measured from wave field of an absorptive finely layered sequence (case (d)), because it is the case in which both stratigraphic filtering and absorption contribute to the overall amplitude attenuation and dispersion. For each well, I computed how the measured first-order entropy changed from wave field (a) to wave field (d), and compared the change with the strength of intrinsic Q and extrinsic Q in wave field (d) estimated by the spectral ratio method, to see if the change responses to the different relative strength of intrinsic and extrinsic Q regularly. Analysis in previous chapter suggests that, for the first-order entropy, the inclusion of extrinsic Q in the wave field tends to increase the entropy peak value, whereas the inclusion of intrinsic Q in the wave field is likely to reduce the entropy peak value.

As many wells as possible (in our case, all seven wells) are included in the experiment to ensure that the result reflects the character of the information measure rather than the data. The collection of seven wells is by no means large but it can at least give us an overall idea of how the interrelation of entropy peaks of case (d) and (a) is related to different Q strength.

4.2 Spectral ratio method

4.2.1 Theoretical review

A variety of methods exist in time and frequency domain aiming at estimating Q in the wave field, such as the spectral ratio (Bath, 1974), wavelet modelling (Jannsen et al., 1985) and dominant frequency (Margrave, 2017). I applied the spectral ratio, the widely used and one of the most reliable methods of Q determination, to my experiment to measure the attenuation in wave field (d) built from the wells.

The method works as follows. In a VSP data set, let $A_x(f)$ be the amplitude spectrum of a downhole pulse recorded at depth x and $A_0(f)$ be the amplitude spectrum of the reference downhole pulse recorded at depth x_0; the relationship between the two amplitude spectra is:

$$A_x(f) = G_x A_0(f) e^{-B_x f}. \tag{4.1}$$

The equation describes the process of the pulse being attenuated in amplitude when it propagates from depth x_0 to depth x (generally $x > x_0$). G_x and B_x are both independent of frequency, but they represent different aspects of the total attenuating effects. G_x represents attenuating factors such as geometrical spreading, transmission loss, change of geophone settings, etc.. And B_x produces the attenuation effect which is positively related to frequency. Attenuation associated with B_x includes absorption and stratigraphic filtering.

B_x is usually referred to as the cumulative attenuation (CA) from depth x_0 to x. To reflect the average attenuation level in this depth range, define an interval attenuation k_x as:

$$k_x = \frac{B_x}{x - x_0}, \tag{4.2}$$

and it is generalized to

$$k_x = \frac{\Delta B}{\Delta x} \tag{4.3}$$

in case of inconsistent Q distribution with depth.

In equation 4.3, k_x represents the attenuation at depth x, however it is not the attenuation related to quality factor Q in a conventional sense. Recalling the expression of "constant Q theory" (Aki and Richards, 1980):

$$A_x(f) = A_0(f)e^{-\frac{\pi f \Delta t}{Q}}. \tag{4.4}$$

Drawing an analogy between equation 4.4 and 4.1, it is found that:

$$B_x = \frac{\pi \Delta t}{Q} \Rightarrow \frac{B_x}{\Delta t} = \frac{\pi}{Q} = \alpha_x, \tag{4.5}$$

also

$$k_x = \frac{\Delta B}{\Delta x} = \frac{\Delta B}{\Delta t v_x} = \frac{\alpha_x}{v_x}. \tag{4.6}$$

α_x is related to Q, and it has unit $nepers/wavelength$. To calculate α_x, we need to know B_x. If we take the logarithm on both sides of equation 4.1 and reorganize, it is transformed to:

$$\log \frac{A_x(f)}{A_0(f)} = -B_x f + \log G_x. \tag{4.7}$$

We see in equation 4.7 that B_x is the negative of the slope of a linear function of spectral ratio in frequency, and α_x can then be derived according to equation 4.5 or 4.6. In practice, the reference amplitude spectrum A_0 is usually chosen at early traveltime where attenuation has not taken place, so that α_x at any depth x in reference to this A_0 will be the true attenuation value in situ, rather then a relative quantity.

4.2.2 Q determination in seven wells

When applying the spectral ratio method to the wave field, there are aspects which must be addressed in order to ensure a reliable outcome:

(1) The spectral ratio method has resolution limit no smaller than several hundred feet due to the inconsistency of source wavelet and interference from upgoing waves (Hauge, 1981). Thus in this experiment, B_x is linearly fitted over a large depth interval (>50m) to get Q information;

(2) It is advisable not to use information over the entire frequency range when extracting B_x from the linear function of spectral ratio versus frequency. Empirically, both the low and high frequency portions of the amplitude spectrum are dominated by noise, rather than signal. Because of that, B_x should be extracted from a limited frequency range which lies around the dominant frequency of seismic waves. By checking the amplitude spectrum of traces in the wave fields, I decided that the trustworthy frequency range for all wells is 10-100Hz.

With these aspects taken into account, I applied the spectral ratio method to two kinds of wave field built from seven wells: one has identical subsurface features as case (d) in figure 3.4—an absorptive finely layered sequence; the other, as a reference, share subsurface features of case (c) in figure 3.4—an absorptive slab. In this case, they were built using quality factor $Q = 70$ for all depths instead of $Q = 20 - 200$ as was used in building the figure 3.4 wave fields to simplify the Q estimation. I will still refer to them as case/wave field (d) and case/wave field (c) in this experiment.

The Q estimated from case (c) (intrinsic Q) contains only intrinsic Q and that estimated from case (d) (apparent Q) contains both intrinsic and extrinsic Q. Considering that wave field (d) is identical to wave field (c) in every other aspects except the additional inclusion of internal multiples, I took the Q estimated from (c) as the intrinsic Q in (d). Intrinsic Q and apparent Q have the relationship (Spencer et al., 1982):

$$\frac{1}{Q_{apparent}} = \frac{1}{Q_{intrinsic}} + \frac{1}{Q_{extrinsic}}. \tag{4.8}$$

From equation 4.8, the extrinsic Q strength and its percentage in total Q of case (d) can be derived. Figure 4.1 is presenting the apparent Q and intrinsic Q distribution estimated from wave fields of well Blackfoot 1227 as an example. Estimated Q information of all wells is listed in table 4.1 and 4.2.

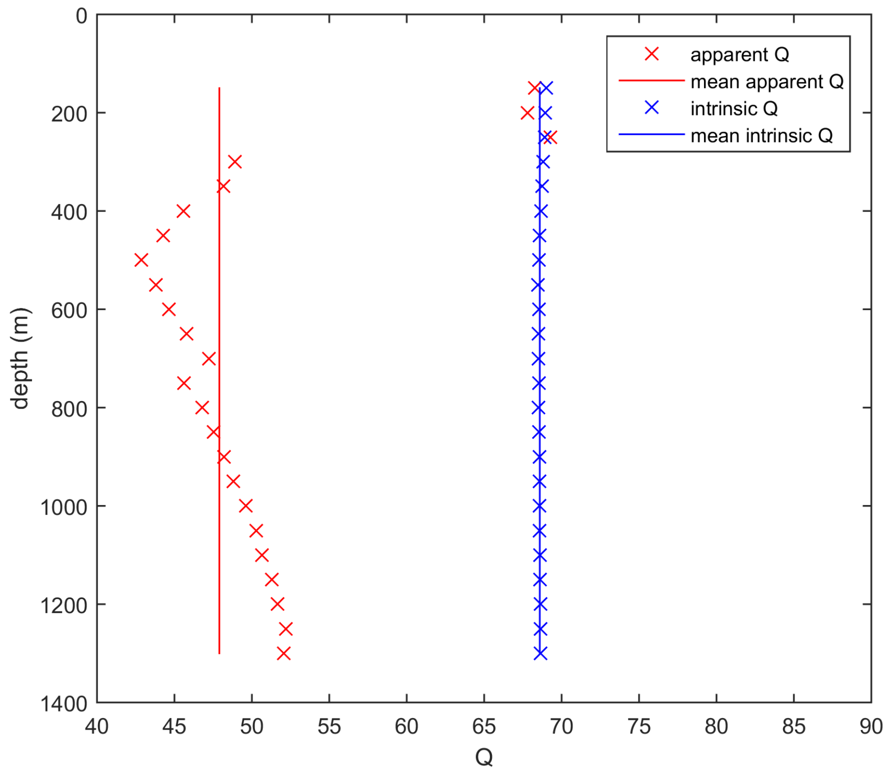

Figure 4.1: Intrinsic and apparent Q distributions with depth of case (c) and case (d) in figure 3.4 computed by spectral ratio method.

Seen in figure 4.1 and table 4.1, the measured intrinsic Q for well Blackfoot 1227 is 68.6, very close to $Q = 70$ that was used when generating synthetic data sets. And the measured apparent Q deviates from its mean value at different depths. These features of measured Q values are shared by other six wells so their Q distributions are not presented. Since I intend only to get a general idea of the relative strength of intrinsic and extrinsic Q in the well positions, also, the entropy value measured from a time snapshot includes a mix of Q effects of all depths, the Q distribution over small depth interval is not needed. Therefore, mean values of Q are adopted for the experiment.

Table 4.1: Q information in seven wells' positions (I)

	Roemer Bell No. 1-1	Kissel A No. 1-8	Blackfoot 1227	Blackfoot 1409
Intrinsic Q	68.6	68.6	68.7	68.5
Apparent Q	29.2	54.2	47.9	35.8
Percentage of extrinsic Q in total Q (%)	57	21	30	48

Table 4.2: Q information in seven wells' positions (II)

	Hussar 12-27-25-21	Hussar 14-27-25-21	Hussar 14-35-25-21
Intrinsic Q	68.6	68.6	68.7
Apparent Q	47.9	34.1	42.0
Percentage of extrinsic Q in total Q (%)	30	50	39

4.3 Relating the entropy behavior to the strength of extrinsic Q

The last row of table 4.1 and 4.2 lists how much of the total Q is contributed by the extrinsic Q. To find out the connection between entropy behavior and attenuation strength, I compared the extrinsic Q strength with the entropy peak increase from case (a) to (d) for different wells. A positive entropy peak increase indicates that wave field (d) contributes to a larger entropy peak value than (a) and negative number indicates a smaller entropy peak value of wave field (d) than (a). Also, the larger the number, the more the entropy peak increases from (a) to (d). I only investigated the first-order entropy in this experiment, so every "entropy peak increase" mentioned in the following content means the peak increase of the first-order entropy. The comparison between entropy peak increase and extrinsic Q strength in total Q of seven wells is displayed in figure 4.2.

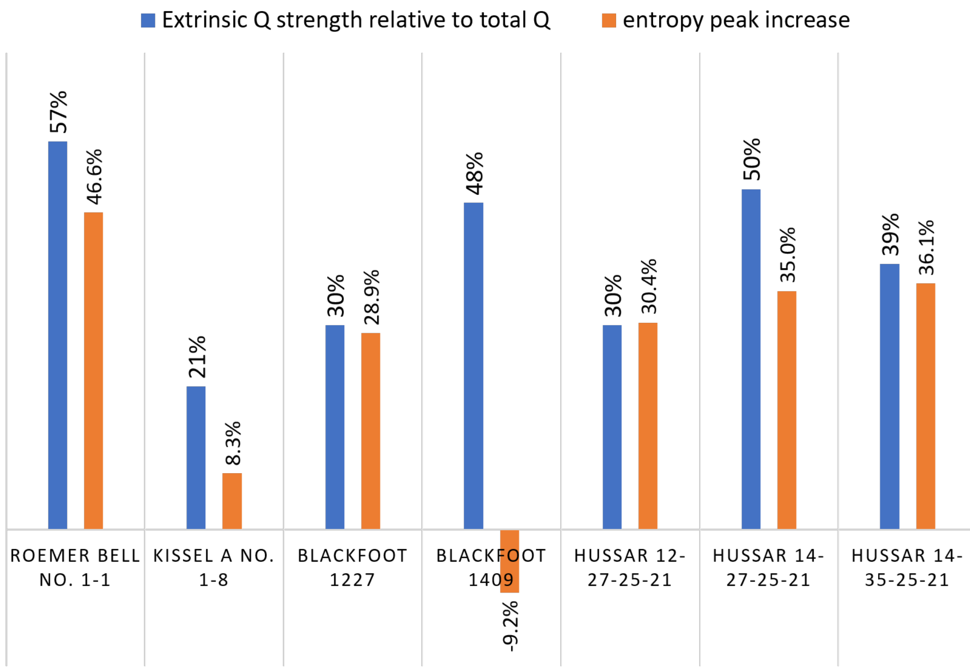

Figure 4.2: Comparison between extrinsic Q strength relative to total Q and the entropy peak increase from case (a) to case (d) of seven wells.

Basing on existing knowledge of time domain first-order entropy, I speculate that the stronger the strength of extrinsic Q in total Q is, the larger the entropy peak increase will be. This speculation is somehow supported by figure 4.2. Roemer Bell No. 1-1, the one having the strongest extrinsic Q of all wells, also has the largest entropy peak increase of all; in contrast, Kissel A No. 1-8 appears to have the weakest extrinsic Q and the smallest entropy peak increase. A similar positive relationship of extrinsic Q strength and the entropy peak increase is observed on well Blackfoot 1227 and three wells from Hussar working area as well. Despite that these six wells show good similarity, it is hard not to notice the abnormal behavior of well Blackfoot 1409. It has the third strongest extrinsic Q but the smallest entropy peak increase (actually negative).

The abnormality of Blackfoot 1409 may be due to a poorly estimated extrinsic Q strength or an undiscovered character of entropy. To find the answer, I reviewed and compared log data for the seven wells. Figure 4.3 displays the P-wave velocity and density logs of all wells, zooming on the depth region 400-600m. Obvious peculiarity was found in (4)—log data of Blackfoot 1409. First, they seem to have a narrower frequency band than log data of other six wells. Figure 4.4 verifies it. We see that wave field (c) for Blackfoot 1409 has a narrower frequency band than that of Blackfoot 1227, with the partial loss of both high and low frequency components. This would almost certainly have affected the outcome of spectral ratio method, since there will be fewer points corresponding to signal when linearly fitting the spectral ratio to frequency using equation 4.7.

Second, the velocity and density distributions of Blackfoot 1409 show little detail in small depth range due to the lack of high frequency information, and they do not have the cyclic feature that log data of other wells have. So that the interbed reverberations in wave fields built from these logs may not be as strongly developed as in other wells and thus have a weaker extrinsic Q effect on the entropy peak value. To demonstrate the point, I computed the transmission loss (TL) exhibited by the wells, since transmission loss and external cumulative attenuation are usually positively related (Schoenberger and Levin, 1978). If Blackfoot 1409 has a smaller transmission loss than others, is should also has a weaker extrinsic Q. The one-way transmission loss of a normal incident wave with $amplitude = 1$ recorded by the bottom receiver (at 1300m) was computed, according to:

$$one-way\ transmission\ loss = 1 - \prod_{k=0}^{N}(1 - R_k). \tag{4.9}$$

In which N is the total number of layers through which the wave has transmitted, R is the reflection coefficient of the kth interface.

One-way transmission loss in the depth range 0-1300m for seven wells are listed in table 4.3. It turns out that the value of Blackfoot 1409 is significantly smaller than others, being only half of the largest value. Thus it is reasonable to say that this well has the weakest extrinsic Q among all. As a result, it should have the smallest entropy peak increase.

To sum up, the reason that Blackfoot 1409 failed to show the positive relation between extrin-

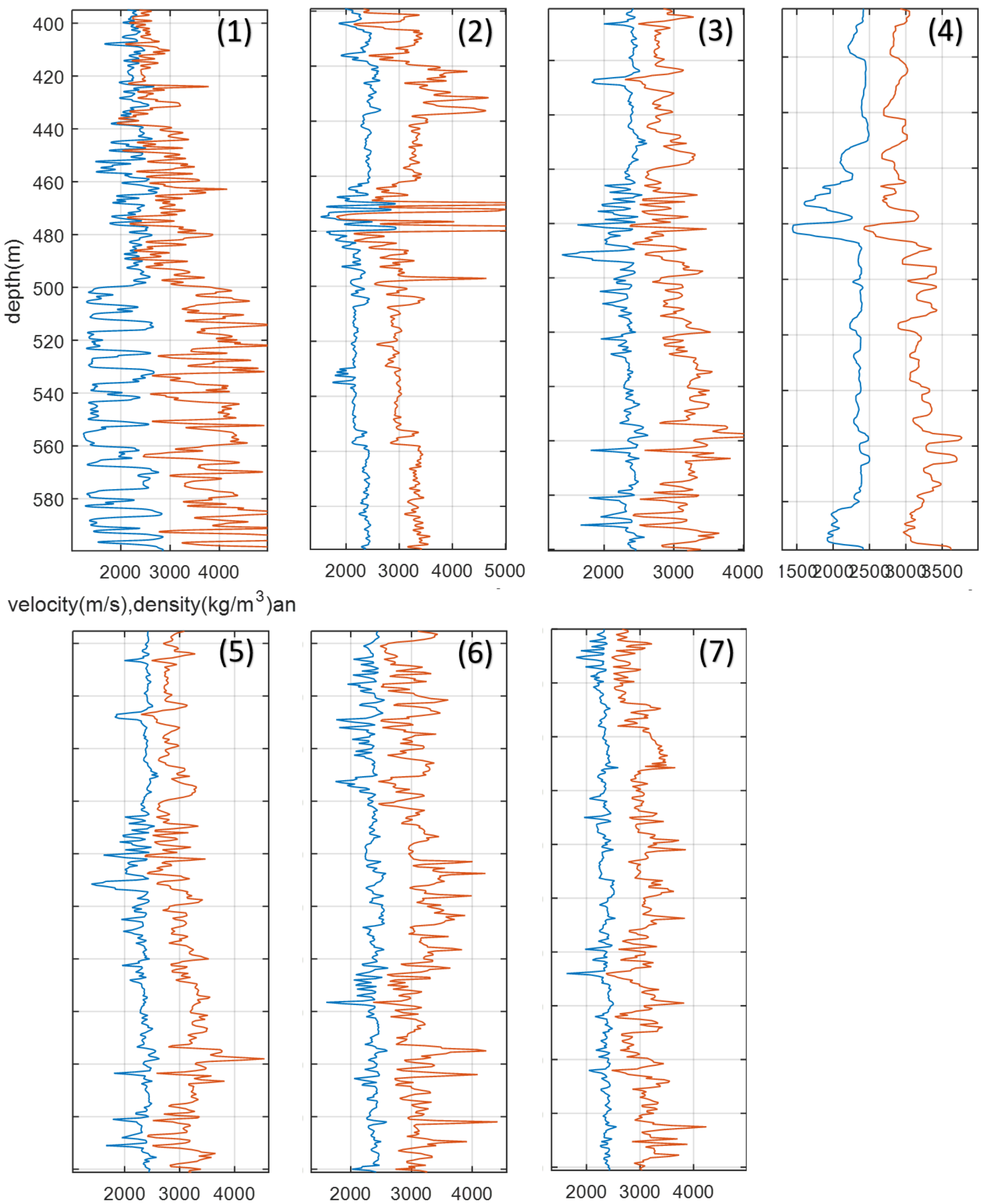

Figure 4.3: P-wave velocity and density logs in depth range 400-600m of well: (1) Roemer Bell No. 1-1; (2) Kissel A No. 1-8; (3) Blackfoot 1227; (4) Blackfoot 1409; (5) Hussar 12-27-25-21; (6) Hussar 14-27-25-21; (7) Hussar 14-35-25-21.

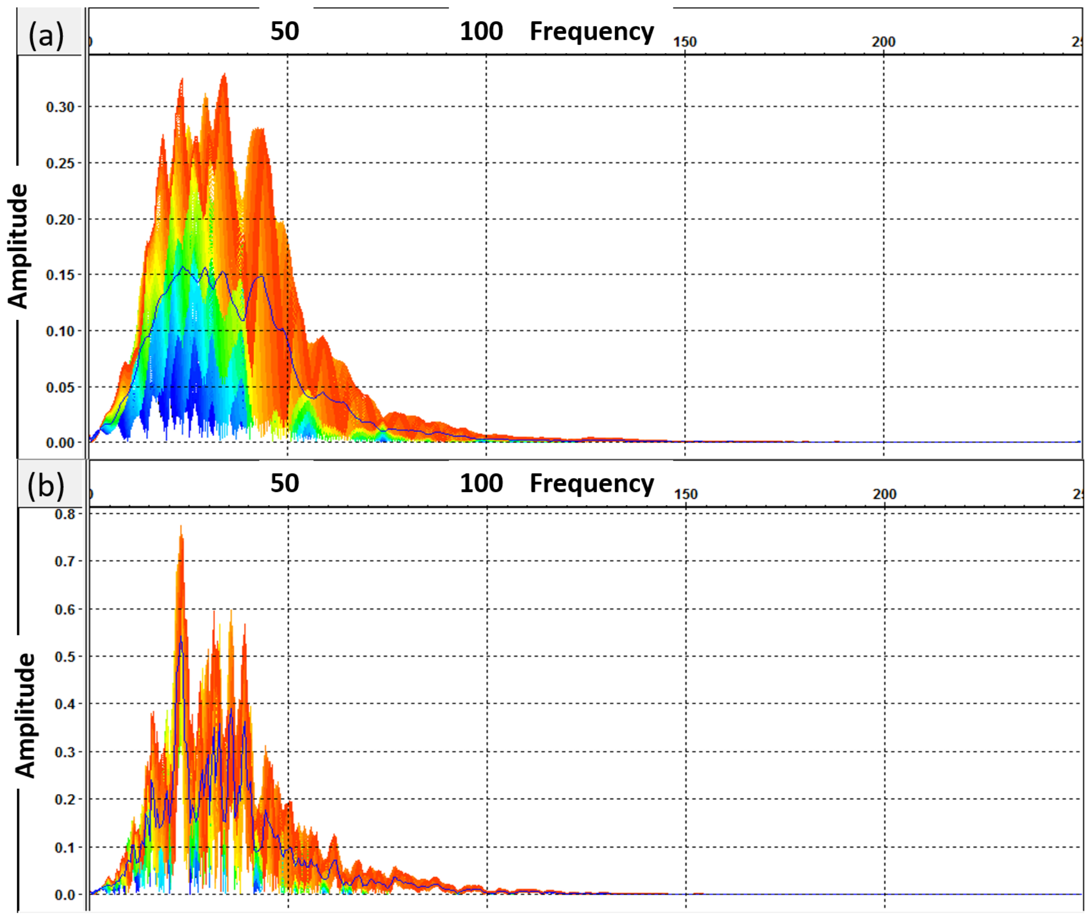

Figure 4.4: Frequency bands of wave field (c) built from well Blackfoot 1227 (a) (figure 3.4) and Blackfoot 1409 (b).

sic Q strength and entropy peak increase as other wells did is very likely that its Q was poorly estimated by the spectral ratio method.

Table 4.3: One-way transmission loss of seven wells

	Roemer Bell No. 1-1	Kissel A No. 1-8	Blackfoot 1227	Blackfoot 1409	Hussar 12-27-25-21	Hussar 14-27-25-21	Hussar 14-35-25-21
TL	0.99	0.97	0.86	0.51	0.86	0.88	0.86

4.4 Chapter summary

The experiment in this chapter showed promise for utilizing an information measure on the wave fields for estimating the relative strength of intrinsic Q and extrinsic Q when they both affect the seismic wave. Among seven wells that were tested, six exhibited good agreement with the hypothesized relationship of extrinsic Q strength relative to total Q and the entropy peak increase from wave field (a) to wave field (d) built from the wells. Specifically, the stronger extrinsic Q is relative to total Q, the larger the entropy peak increase would be.

In figure 4.2, all wells except Blackfoot 1409 appear to have positive entropy peak increase, when extrinsic Q strength in their positions ranges from 20% to 60%. It indicates that the impact of extrinsic Q on entropy is more influential than that of intrinsic Q. When both Q take 50% of total attenuation, the entropy peak of wave field (d) is larger than that of wave field (a), instead of being comparable. Therefore, I provisionally conclude that whenever the entropy peak increase is negative, it could mean that the extrinsic Q strength over the depth interval of interest is considerably weak, likely to take less than 20% of total attenuation.

Chapter 5

INFORMATION MEASURE ON A FIELD VSP DATA SET

5.1 Chapter overview

The previous two chapters focused on the information measure of the synthetic data. However, the situation is likely simpler for synthetic data than for real data, mainly due to the absence of many kinds of interference (surface-related multiples, noise from environment and acquisition equipments, etc.) in synthetic data. These interferences tend to increase the disorder in the wave field and make the seismic events less well distinguished by the amplitude bin. Thus I wonder if the information measurement will be as definitive when applied to more complex real VSP data.

In this chapter, the entropy calculation procedures developed and validated in the previous chapters are partially repeated and applied to a real VSP data. I applied the first-order entropy calculation to four different real VSP data sets, in which the internal multiples and absorption are selectively eliminated/compensated by appropriate seismic processing, to form a similar controlled trial as for the synthetic data, then used the entropy variation results of the data sets to estimate the extrinsic Q strength of the region.

5.2 Data set

Experiments of this chapter use the zero-offset record of a multicomponent walkaway VSP dataset (Hall et al., 2012). CREWES participated in the data acquisition in 2011. The location and the identity of the company are not disclosed by request. Data from this area are suitable for the stratigraphic filtering study because well logs acquired at a nearby position reveal good layering character, and comparison between log data and the simulated wavelet implies that the stratification of the area is nonresolvable (figure 5.1). Nevertheless, the stratification does not seem to have an apparent cyclic feature, from which a weak stratigraphic filtering effect should be expected.

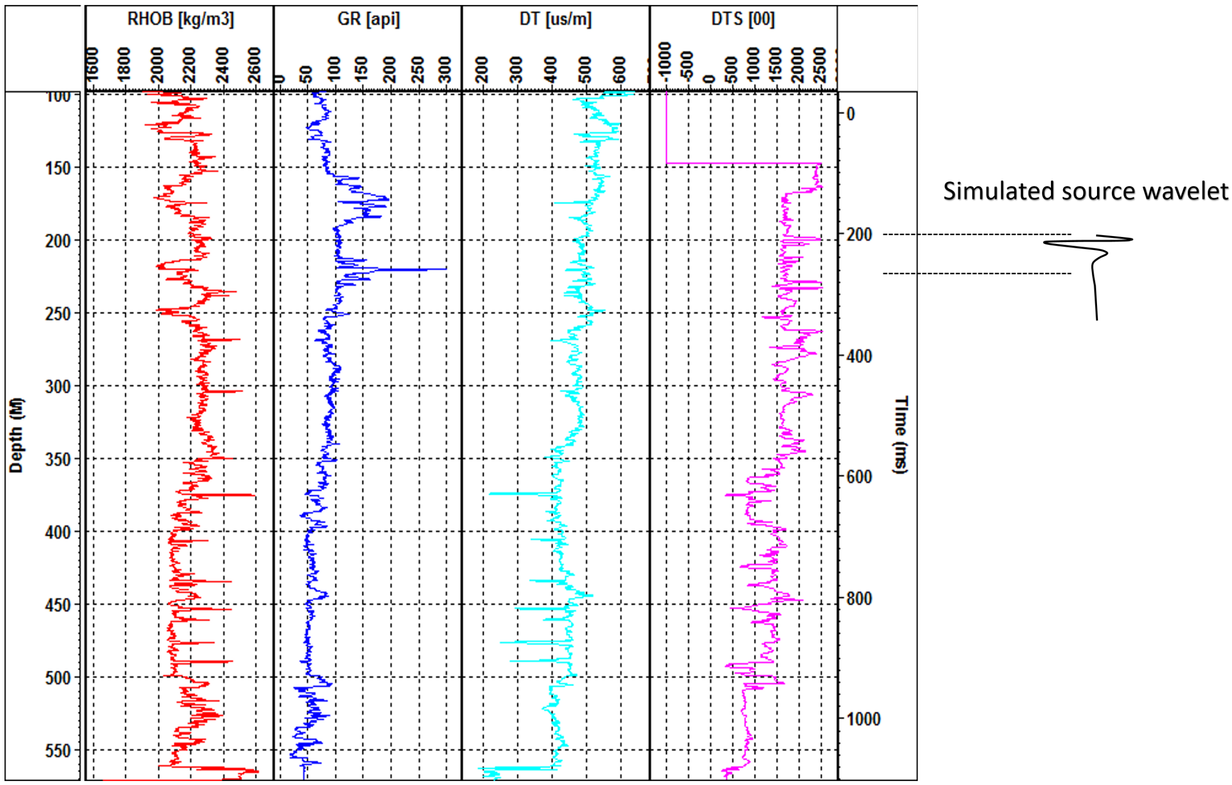

Figure 5.1: Log data from a nearby well position of the VSP data used in the research, and its comparison with the simulated source wavelet.

5.3 First-order entropy calculation on real VSP data

5.3.1 Calculation strategy

A controlled trial consisting of four wave fields including various attenuating factors was designated for the information measure. The wave fields contain, respectively, attenuating effects of: a) neither absorption nor stratigraphic filtering ; b) stratigraphic filtering only; c) absorption only; and d) both absorption and stratigraphic filtering.

To get the wave fields, the raw zero-offset VSP record was pre-processed to preferentially eliminate the undesired attenuating factors. Seen in Figure 5.2, the record has satisfactory S/N ratio, and P-wave events such as primaries, surface-related multiples, internal multiples can be recognized. S-wave events in the record are ignored, because the wave type does not really matter in the information measure and the S-wave energy is quite weak compared to the P-wave energy.

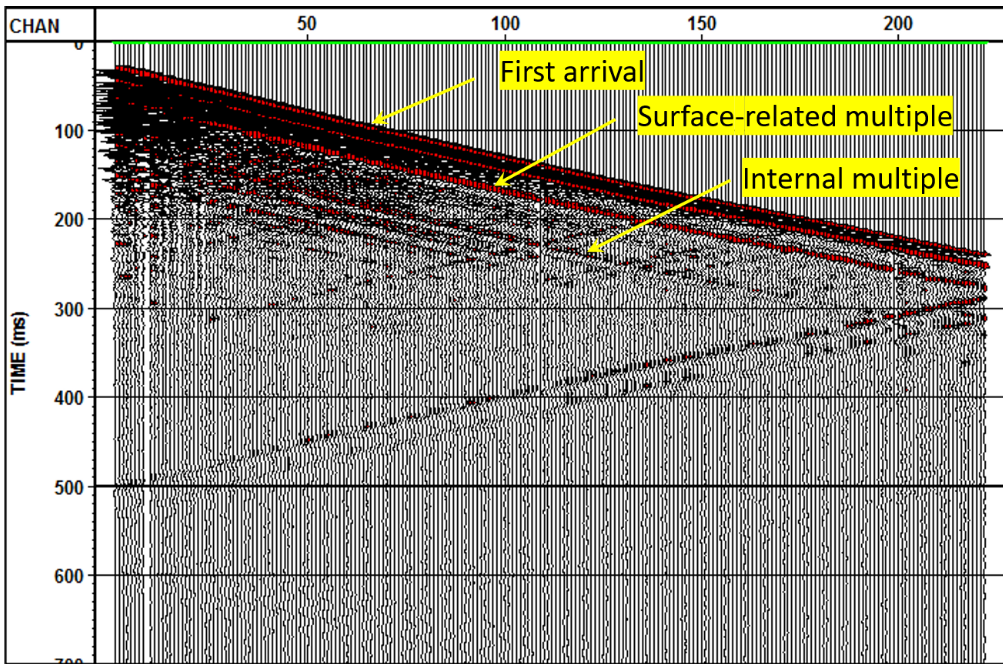

Figure 5.2: The zero-offset VSP record of an anonymous multicomponent walkaway VSP data set.

To prepare the data for the controlled trial, I used a 3.2 exponential gain to compensate the absorptive attenuation based on the record's intrinsic Q estimated by the spectral ratio method (detail is in following section), this way the absorption will not be overly or insufficiently compensated in general. I used predictive deconvolution to remove surface-related multiples and internal multiples in the record. The pre-processing went like this: a predictive deconvolution was first applied to the record to remove source ghost. This generated wave field (d). Then I applied a 3.2 exponential gain to (d) to get wave field (b). Meanwhile, I applied another predictive deconvolution to wave field (d) to eliminate the internal multiples in the field to get (c). To get wave field (a), both the exponential gain and the internal-multiple-eliminating predictive deconvolution were applied to wave field (d). Figure 5.3 and 5.4 show the processed wave fields. Most parts of the four wave fields hold decent S/N ratio except the near surface zone; thus data from the first 30 traces were discarded in the information measure.

5.3.2 Results

The time domain first-order entropy calculation was applied to the VSP records using the first-order entropy algorithm in chapter 3. Amplitude bin size used is 0.001. Comparison of entropy variation results for the four wave fields is displayed in figure 5.5.

Focusing on the rising portion of the entropy curves, it can be seen that:

(1) Wave fields including internal multiples contribute to entropies with larger peaks than entropies calculated from wave fields excluding internal multiples, seen by comparing red and purple curves to the blue and yellow ones respectively;

(2) Derived from wave fields which include absorption, the yellow and purple entropy curves have smaller peaks than red and blue ones;

(3) Overall, the most disordered wave field contributes to the largest entropy (red curve) and the least disordered wave field contributes to the smallest entropy (yellow curve).

Intrinsic Q and extrinsic Q have opposite effects on the entropy variation result, just like in the synthetic data experiment. I then examined the possibility that one could use this measured entropy result to predict the extrinsic Q strength relative to total Q in this region.

5.4 Estimation of extrinsic Q strength of the region

A negative entropy peak increase from wave field (a) entropy to wave field (d) entropy can be derived from figure 5.5. The number being negative implies that extrinsic Q strength of the region is considerably weak, accounting for less than 20% of the total attenuation strength.

I measured the Q strength in wave field (c) and (d) of figure 5.4 with the spectral ratio method as a reference. Amplitude spectrum information of 10-250Hz was utilized because the raw VSP

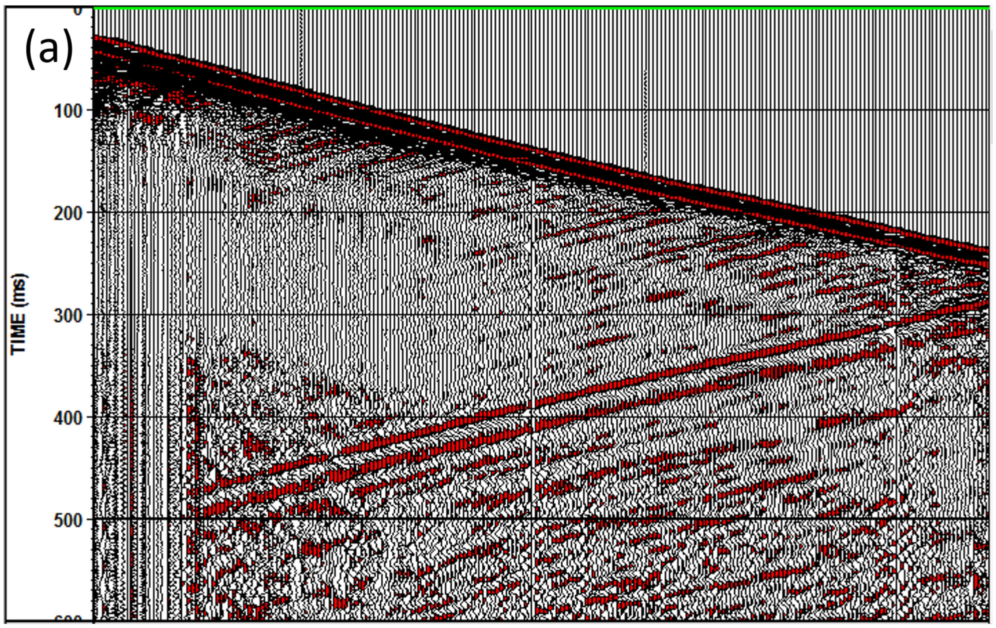

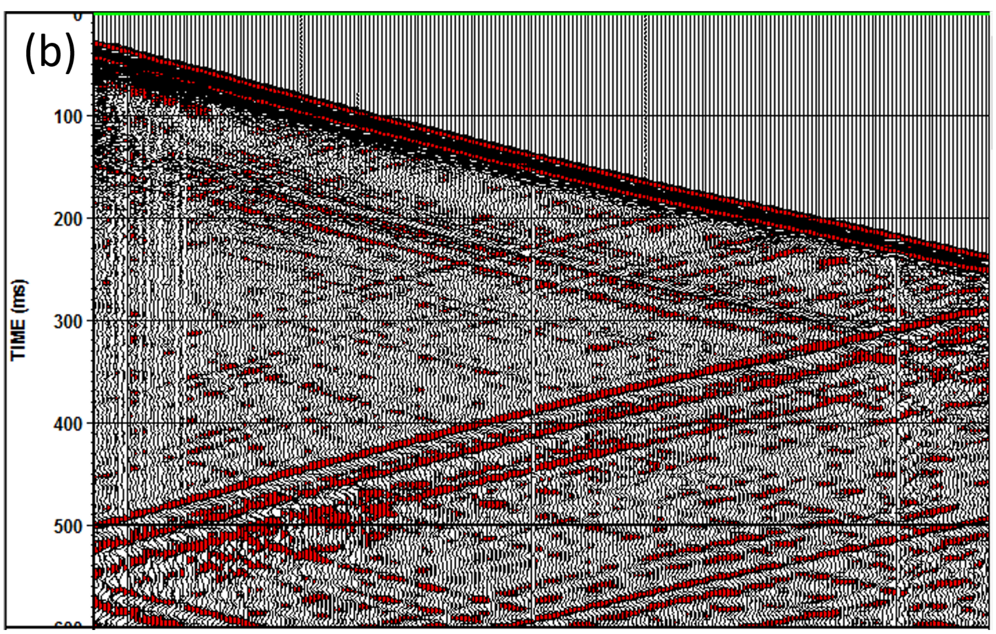

Figure 5.3: Processed zero-offset VSP records. (a) is obtained by applying a 3.2 exponential gain and two passes of predictive deconvolution (aiming at removing source ghost and internal multiples) to figure 5.2 record; (b) is obtained by applying a 3.2 exponential gain and one time of predictive deconvolution (aiming at removing source ghost) to figure 5.2 record.

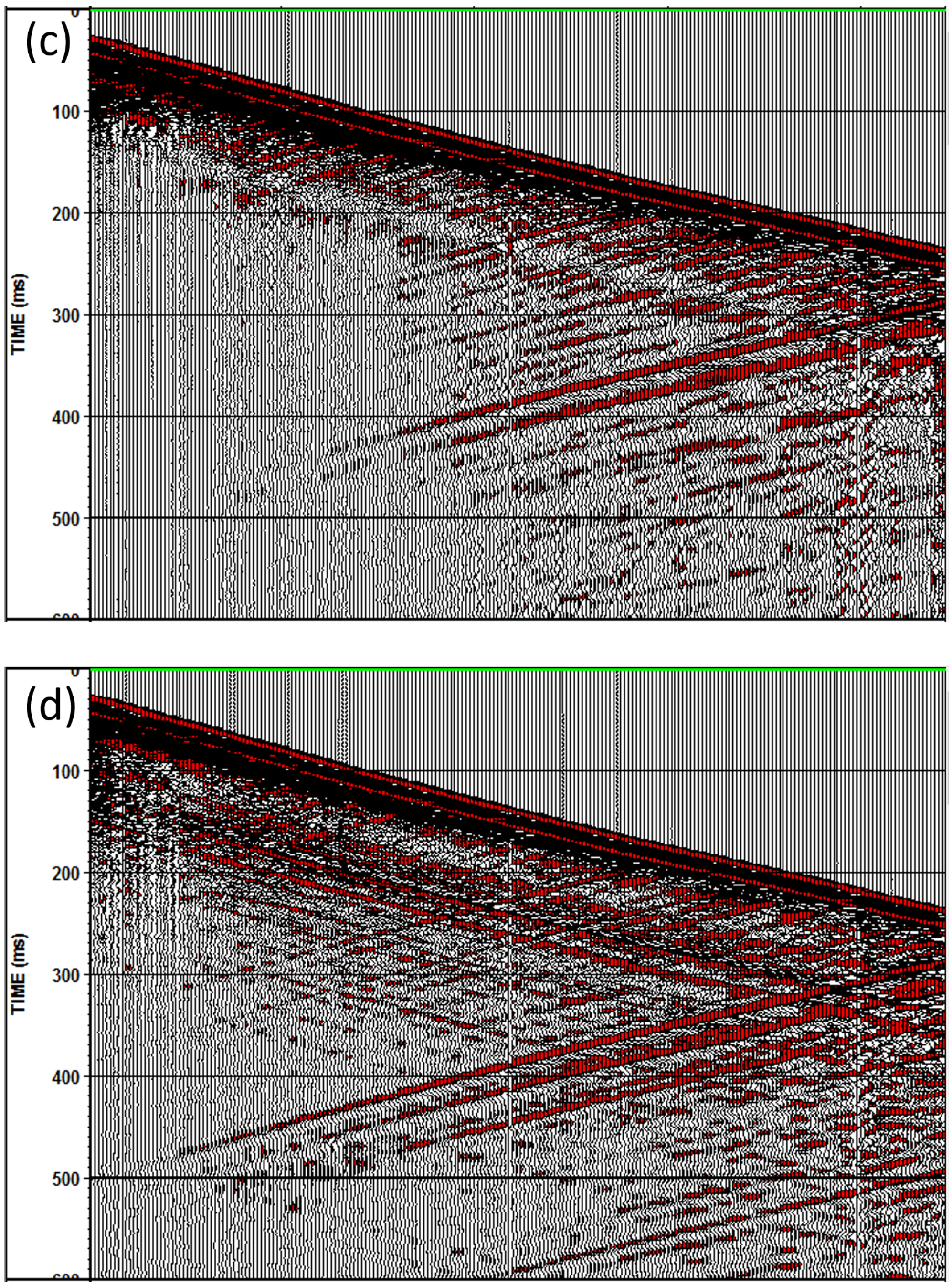

Figure 5.4: Processed zero-offset VSP records. (c) is obtained by applying two passes of predictive deconvolution (aiming at removing source ghost and internal multiples) to figure 5.2 record; (d) is obtained by applying one time of predictive deconvolution (aiming at removing source ghost) to figure 5.2 record.

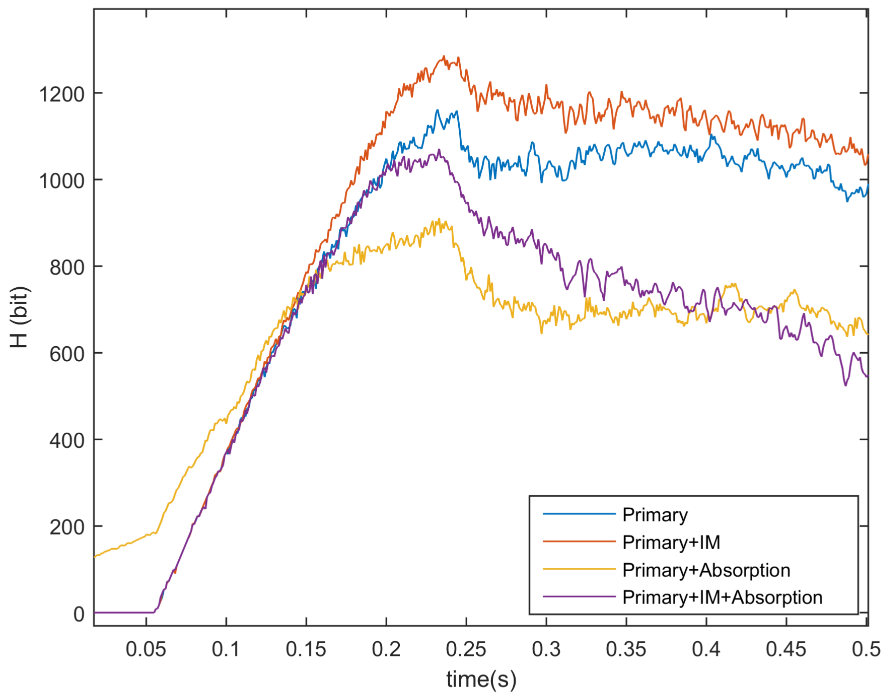

Figure 5.5: The first-order entropy variation result for wave fields in figure 5.3 and 5.4 (zooming on time 0-0.5s).

record has a broad frequency band (figure 5.6). Figure 5.7 and 5.8 show the measured intrinsic and apparent cumulative attenuation (CA) B_x from wave field (c) and (d) respectively. The final α_x is displayed in figure 5.9, with detailed information listed in table 5.1. Seen in table 5.1 that extrinsic Q accounts for approximately 15% of the total Q in this region.

The extrinsic Q strength, implied by the entropy behavior and calculated from the attenuation determination method, agrees with each other.

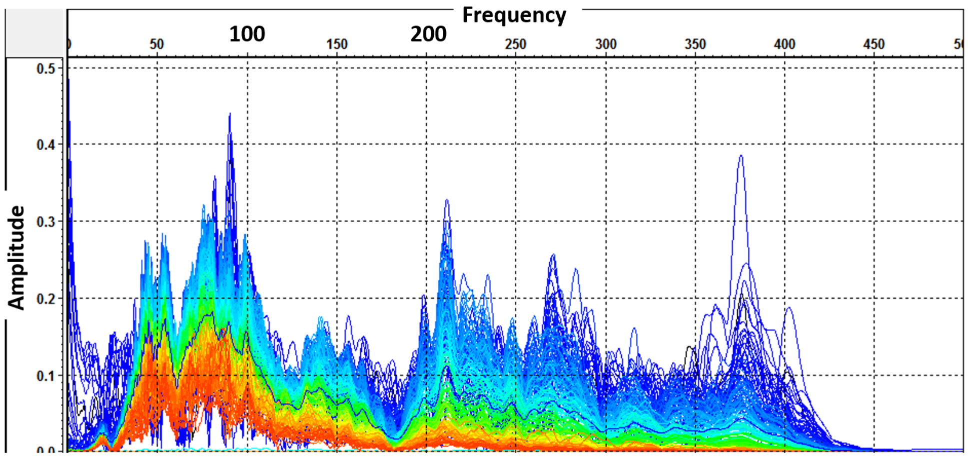

Figure 5.6: Frequency band of the VSP record in figure 5.2.

Table 5.1: α_x distribution information of the anonymous Canadian heavy oil reservoir

Depth range (m)	120-328	330-502
Intrinsic α_x $(nepers/wavelength)$	0.069	0.080
Apparent α_x $(nepers/wavelength)$	0.080	0.094
Percentage of extrinsic α_x in total α_x (%)	15	15

5.5 Chapter summary

Intrinsic and extrinsic Q have opposite effects on the measured entropy of the field VSP data. And the extrinsic Q strength estimated from the entropy behavior supports the speculation made at the end of chapter 4, that when the entropy peak of a wave field (d) which contains both intrinsic Q

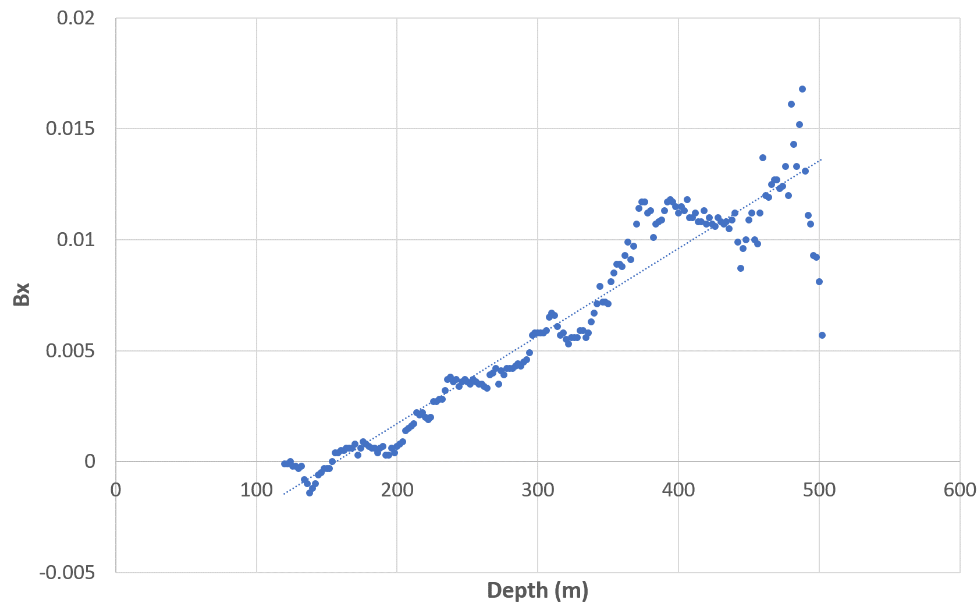

Figure 5.7: CA distribution with depth of wave field (c) in figure 5.4.

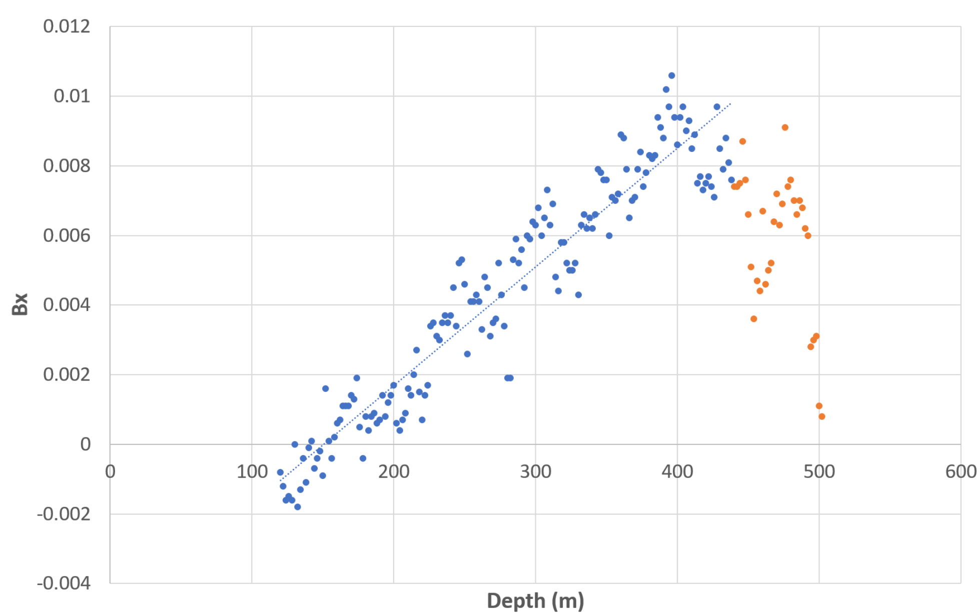

Figure 5.8: CA distribution with depth of wave field (d) in figure 5.4. Orange points are abandoned when linear fitting B_x for k_x.

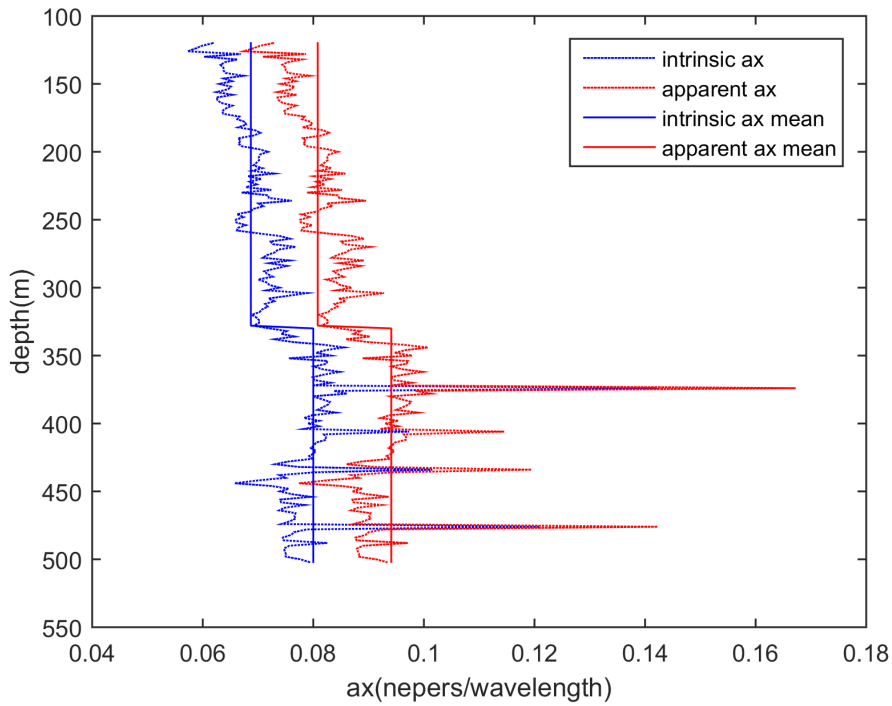

Figure 5.9: α_x distribution with depth of of wave field (c) in figure 5.4 (blue) and of wave field (d) in figure 5.4 (red). Solid lines show their mean values.

and extrinsic Q effects is smaller than the entropy peak of a wave field (a) which is identical to (d) in every other aspects but contains no frequency-dependent attenuation, it is implied that the extrinsic Q strength in the studied region is considerably weak and possibly accounts for less than 20% of the total attenuation strength.

The real VSP data I used has a good S/N ratio, so the information measure was able to present results that were expected. However, this brings up the thought that, for real data that has poor S/N ratio, whether or not the information measure is going to be as efficient needs further investigation.

Chapter 6

CONCLUSIONS

My research studied the similarities and differences between the intrinsic Q and extrinsic Q. These two processes affect seismic waves almost identically, but have different physical mechanisms. Intrinsic Q describes the wave energy dissipation due to rock properties, while extrinsic Q is related to energy scattering caused by internal multiples.

The advantage of using information measure (Shannon entropy), is that we can therefore investigate the energy disorder inside the wave field caused by amplitude attenuation and dispersion and monitor the change of disorder with wave propagation (with time), using the designed research scheme. Experiments in this research show that entropy serves as a "magnifier". It enhances the process difference between internal and external attenuation, and displays the difference in a visible, measurable form. The first-order and second-order entropy calculations in time domain information measure, although having divergent outcomes, convey the same idea that, when a proper amplitude bin size is chosen, entropy gives opposite responses to absorption and internal multiples. Specifically, internal multiples tend to raise the entropy curve upward and absorption is more likely to pull the entropy curve downward. I also showed that this opposite response of entropy might be utilized to estimate the relative strength of intrinsic Q and extrinsic Q in a wave field in a scenario that they are both active.

The information measure devised in this research has limitations, though. First, the entropy response is sensitive to the amplitude bin size used in the calculation. A change of amplitude bin size would almost definitely give rise to a change in the entropy response, while the size of the effect is unknown. This adds uncertainty to the approach. Second, Shannon entropy is a qualitative measurement of the seismic wave field, means that there are no definite relationships between it and seismic attributes. So that one entropy peak increase is not enough to let us determine the extrinsic

Q of the wave field, it needs to be compared with the entropy peak increase from the data sets with known extrinsic Q, as in chapter 4. Considering that the measured entropy result is affected by the data quality, for data sets, especially the field data sets, that are uneven in quality (e.i. S/N ratio), the comparison among their information measure results will be unreliable. According to this, it is suggested that the information measure be conducted only on synthetic data sets, as a supplement of the field VSP studies.

Seven well logs and a real VSP data set are tested in this research. Although this is far from enough to confirm the universal applicability regarding this information measure, the results show promise in assisting stratigraphic filtering analysis.

Appendix A

DEFINITION OF INTRINSIC Q

In the case that seismic wave propagates in an anelastic media, the wave amplitude is attenuated by the internal friction of the material, and wave energy is partially transformed into heat. This process is usually referred to as absorption or energy dissipation and is measured by

$$\frac{1}{Q} = -\frac{\triangle E}{2\pi E} \tag{A.1}$$

in which Q is the dimensionless quality factor of the media, E is the maximum energy stored in the wave and $\triangle E$ is the energy loss per wavelength (Aki and Richards, 1980).

Thus, the spatial amplitude attenuation for any plane wave with frequency ω is

$$A_x(\omega) = A_0(\omega) exp - \frac{\omega x}{2cQ} \tag{A.2}$$

with A_x being the attenuated amplitude after wave propagates a distance x, A_0 being the original amplitude and c being the phase velocity (Aki and Richards, 1980). The quality factor Q can be a constant number in the seismic frequency range under some conditions, which is called a constant Q theory.

Besides that, for a causal signal, the attenuation is connected to wave dispersion, where different frequency components of a seismic wave will travel in different velocities (Futterman, 1962).

Appendix B

COMPUTING NUMBER OF EVENTS IN THE WAVE FIELD OF A HORIZONTAL MEDIA WITH AN ABSORPTIVE UPPER BOUNDARY

Consider the wave field generated at normal incidence to a horizontal N-layer media ($N \geq 2$) with an absorptive upper boundary, where each layer is homogeneous inside (figure B.1). If we only take events that have no more than three bounces into account, the downgoing wave field includes the first break and the first-order internal multiples and the upgoing wave field includes the primaries and the second-order internal multiples. As shown in the figure, "P" represents primary, "IM" represents internal multiple and the ordered numbers following the letters represent from which interfaces the event has been reflected successively.

To know the number of upgoing and downgoing events and compare them, the number of each kind of event needs to be calculated. First, the first break excites N primaries at N interfaces. Then, each primary excites a downgoing first-order internal multiple when passing through an interface, so the primary generated by the mth interface excites first-order internal multiples at $m-1$ interfaces above it, excluding the surface. In total, there are $\sum_1^N (m-1)\,(m\ is\ the\ variable)$ first-order internal multiples in the field. The generation of the second-order multiples is similar, that the first-order multiples excite it when passing through interfaces below which the first-order multiples are generated from. Each $IM_{mb}\,(m = 1,2,\ldots,N; b = 1,2,\ldots,m-1)$ will excite $N-b$ second-order internal multiples, in total there are $\sum_1^{m-1}(N-b)(b\ is\ the\ variable; m = 1,2,\ldots,N)$ second-order internal multiples in the field.

Now, the total number D of downgoing events in the wave field is

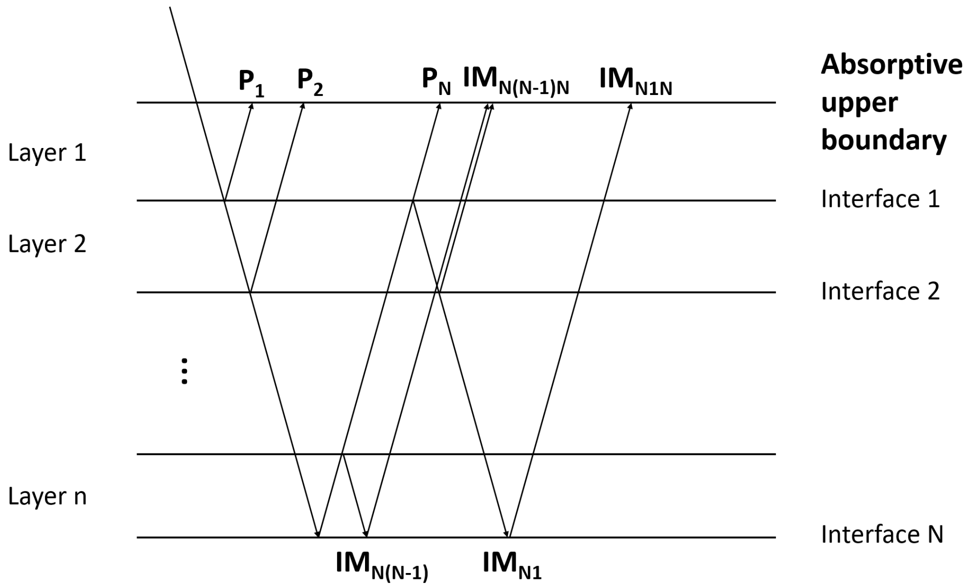

Figure B.1: Part of the wave field generated from a normal incidence (for better demonstration, wave propagation is not normal to the interfaces in figure) at a horizontally N layered media ($N \geq 2$)with an absorptive upper boundary. Each layer is homogeneous inside.

$$\begin{aligned} D &= \text{num of first break + num of the first-order internal multiples} \\ &= 1 + \sum_{1}^{N}(m-1), \end{aligned} \tag{B.1}$$

and the total number U of upgoing events in the wave field is

$$\begin{aligned} U &= \text{num of primaries + num of the second-order internal multiples} \\ &= N + \sum_{1}^{N-1}(N-b) + \sum_{1}^{N-2}(N-b) + \ldots + \sum_{1}^{1}(N-b). \end{aligned} \tag{B.2}$$

Note that the second part of the equations are actually the same, both are summation from 1 to $N-1$, so

$$U - D = (N-1) + \sum_{1}^{N-2}(N-b) + \sum_{1}^{N-3}(N-b) + \ldots + \sum_{1}^{1}(N-b) > 0. \tag{B.3}$$

There are more upgoing events than downgoing events in the wave field when no surface multiples exist.

Bibliography

Aki, K., and Richards, P. G., 1980, Quantitative seismology:

Banik, N., Lerche, L., and Shuey, R., 1985, Stratigraphic filtering, part I: Derivation of the O'Doherty-Anstey formula: Geophysics, **50**, No. 12, 2768–2774.

Bath, M., 1974, Spectral analysis in geophysics: Developments in solid earth geophysics.

Futterman, W. I., 1962, Dispersive body waves: Journal of Geophysical research, **67**, No. 13, 5279–5291.

Hall, K., Lawton, D., Holloway, D., and Gallant, E., 2012, Tech. rep., CREWES Research Report 24.

Hauge, P. S., 1981, Measurements of attenuation from vertical seismic profiles: Geophysics, **46**, No. 11, 1548–1558.

Hoffe, B. H., Stewart, R. R., Bland, H. C., Gallant, E. V., and Bertram, M. B., 1998, The Blackfoot high-resolution 3-C seismic survey: design and initial results, in SEG Technical Program Expanded Abstracts 1998, Society of Exploration Geophysicists, 103–106.

Innanen, K., 2012, Blurring the line between intrinsic and scattering attenuation by means of the Shannon entropy, Tech. rep., CREWES Research Report 24.

Jannsen, D., Voss, J., and Theilen, F., 1985, Comparison of methods to determine Q in shallow sediments from vertical reflection seismograms: Geophysical Prospecting, **33**, No. 4, 479–497.

Lines, L., Bording, R. P., and Vasheghani, F., 2013, Viscosity estimation using seismic inversion, Tech. rep., CREWES Research Report 25.

Margrave, G., 2017, Seismic-attenuation measures from VSP data by two different methods, in SEG Technical Program Expanded Abstracts 2017, Society of Exploration Geophysicists, 5994–5998.

Margrave, G. F., 2014a, Stratigraphic filtering and Q estimation, Tech. rep., CREWES Research Report 26.

Margrave, G. F., and Daley, P., 2014b, VSP modelling in 1D with Q and buried source, Tech. rep., CREWES Research Report 26.

O'Doherty, R., and Anstey, N. A., 1971, Reflections on amplitudes: Geophysical Prospecting, **19**, No. 3, 430–458.

Qi, Q., Müller, T. M., and Pervukhina, M., 2017, Sonic Qp/Qs ratio as diagnostic tool for shale gas saturation: Geophysics.

Resnick, J., 1990, Stratigraphic filtering: Pure and Applied Geophysics, **132**, No. 1, 49–65.

Richards, P. G., and Menke, W., 1983, The apparent attenuation of a scattering medium: Bulletin of the Seismological Society of America, **73**, No. 4, 1005–1021.

Schoenberger, M., and Levin, F., 1974, Apparent attenuation due to intrabed multiples: Geophysics, **39**, No. 3, 278–291.

Schoenberger, M., and Levin, F., 1978, Apparent attenuation due to intrabed multiples, II: Geophysics, **43**, No. 4, 730–737.

Shannon, C. E., 2001, A mathematical theory of communication: ACM SIGMOBILE Mobile Computing and Communications Review, **5**, No. 1, 3–55.

Spencer, T., Edwards, C., and Sonnad, J., 1977, Seismic wave attenuation in nonresolvable cyclic stratification: Geophysics, **42**, No. 5, 939–949.

Spencer, T., Sonnad, J., and Butler, T., 1982, Seismic Q–stratigraphy or dissipation: Geophysics, **47**, No. 1, 16–24.

Stewart, R. R., Huddleston, P. D., and Kan, T. K., 1984, Seismic versus sonic velocities: A vertical seismic profiling study: Geophysics, **49**, No. 8, 1153–1168.

Trorey, A., 1962, Theoretical seismograms with frequency and depth dependent absorption: Geophysics, **27**, No. 6, 766–785.

Vasheghani, F., and Lines, L. R., 2009, Viscosity and Q in heavy-oil reservoir characterization: The Leading Edge, **28**, No. 7, 856–860.